Alma Mater Studiorum - Università di Bologna

DOTTORATO DI RICERCA IN ASTRONOMIA

Ciclo XXII

Settore scientifico di afferenza: Area 02 - Scienze Fisiche

FIS/05 Astronomia e Astrofisica

LBT AO system: tests and calibration

Presentata da: FRANCESCA PIERALLI

Coordinatore Dottorato
Ch.mo Prof. Lauro Moscardini

Relatore
Ch.mo Prof. Bruno Marano

Dott. Simone Esposito

Esame finale anno 2010

A Golt, a noi.

Contents

Introduction

An Adaptive Optic (AO) system is a fundamental requirement of 8m-class telescopes. We know that in order to obtain the maximum possible resolution allowed by these telescopes we need to correct the atmospheric turbulence. Thanks to adaptive optic systems we are able to use all the effective potential of these instruments, drawing all the information from the universe sources as best as possible.

In an AO system there are two main components: the wavefront sensor (WFS) that is able to measure the aberrations on the incoming wavefront in the telescope, and the deformable mirror (DM) that is able to assume a shape opposite to the one measured by the sensor. The two subsystem are connected by the reconstructor (REC). In order to do this, the REC requires a "common language" between these two main AO components. It means that it needs a mapping between the sensor-space and the mirror-space, called an interaction matrix (IM). Therefore, in order to operate correctly, an AO system has a main requirement: the measure of an IM in order to obtain a calibration of the whole AO system.

The IM measurement is a 'mile stone' for an AO system and must be done regardless of the telescope size or class.

Usually, this calibration step is done adding to the telescope system an auxiliary artificial source of light (i.e a fiber) that illuminates both the deformable mirror and the sensor, permitting the calibration of the AO system. For large telescope (more than 8m, like Extremely Large Telescopes, ELTs) the fiber-based IM measurement requires challenging optical setups that in some cases are also impractical to build. In these cases, new techniques to measure the IM are needed.

In this PhD work we want to check the possibility of a different method of

calibration that can be applied directly on sky, at the telescope, without any auxiliary source. Such a technique can be used to calibrate AO system on a telescope of any size.

We want to test the new calibration technique on the Large Binocular Telescope (LBT) AO system, which is already a complete AO system with the two main components: a secondary deformable mirror with by 672 actuators, and a pyramid wavefront sensor.

1) My *first phase of PhD work* was helping to implement the WFS board (containing the pyramid sensor and all the auxiliary optical components) working both optical alignments and tests of some optical components. Thanks to the 'solar tower' facility of the Astrophysical Observatory of Arcetri, we have been able to reproduce an environment very similar to the telescope one, testing the main LBT AO components: the pyramid sensor and the secondary deformable mirror.

In particular I have worked on the atmospheric dispersion corrector (ADC), checking its behavior by simulations and laboratory tests. Thanks to the good results we are able to implement this element inside the AO optical board.

After some alignment procedures the system has been tested inside the solar tower.

2) Now the *second phase of my PhD thesis*: the measure of IM applying the new technique, called the "sinusoidal modulation technique".

The concept idea of this technique is to introduce a sinusoidal signal with a specific frequency, first selecting a different frequency for each mode (the measured wavefront incoming is decomposed into an orthogonal base of polynomials), and then modulating each mode amplitude with its sinusoidal signal. After this we sum all commands together and apply the summed commands to the DM recording the sensor signal. Finally the main step of the demodulation: the signal of the WFS is demodulated with the different frequencies injected in order to recover the single modes applied. We can apply more than one mode at the same time, operating in open or closed loop indifferently.

In this PhD thesis we have investigated the behavior of this method. Preliminarily we have tested its functionality applying it in a 'classical' way operation, measuring the IM using a fiber auxiliary source to calibrate the system, without any kind of disturbance injected. After that, we have tried to use this

sinusoidal modulation technique in order to measure the IM directly "on sky", so adding an atmospheric disturbance to the AO system. The atmospheric disturbance has been introduced in the optical path by the adaptive secondary unit itself with a disturbance command vector that is added at each loop iteration to the final position command. These measures were made both in simulations (required in order to find the best parameters involved in this calibration method), and in the solar tower system set-up.
The results obtained by this PhD work measuring the IM directly in the Arcetri solar tower system are crucial for the future development: if the acquisition of an Interaction Matrix directly on sky is possible, it means that it will be possible to calibrate an AO system at a telescope class (like ELTs) where the fiber-based IM measure is not possible.

Chapter 1

The LargeBinocularTelescope: LBT

1.1 The need for Adaptive optics

The atmospheric presence is able to distort the wavefront coming from a distance source (i.e a star), because gradients of temperature and velocity determine the conditions for the production of turbulent kinetic energy in the atmospheric layers [Kolmogorov, 1941]. Different temperature layers and different wind speeds give rise to fluctuations in the density of air and therefore in the refractive index of the atmosphere, and distort the light waves leading to distortion of the star image (1.1).

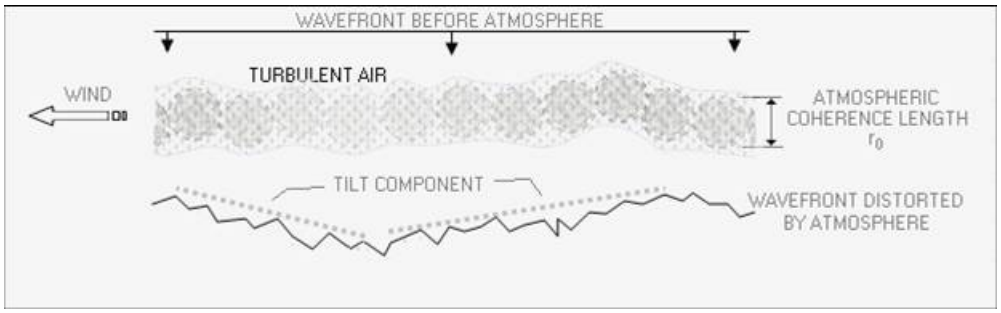

Figure 1.1: Schema of the effect of atmospheric turbulence on the wavefront incoming from a distance source, like a star.

When we are observing with a telescope our image is limited by the angular resolution of this instrument(the smallest angular separation between sources or structures within the image of a single extended source):

$$FWHM \cong \frac{\lambda}{D}(rad) \tag{1.1}$$

The intensity distribution of the image observed is described by the Point Spread Function (PSF). In practice the FWHM of this image is a measure of the astronomical seeing conditions, because the presence of atmosphere gives a factor 100 between the potential and practical resolution, and we are able to obtain only a seeing limited image, where the PSF dimension is characterized by the 'Fried parameter' ([Fried, 1966] that corresponds to the length-scale over which the turbulence becomes significant: 10-20 cm at visible wavelengths at good observatories), and not by the diameter of the telescope (the diffraction limited condition).

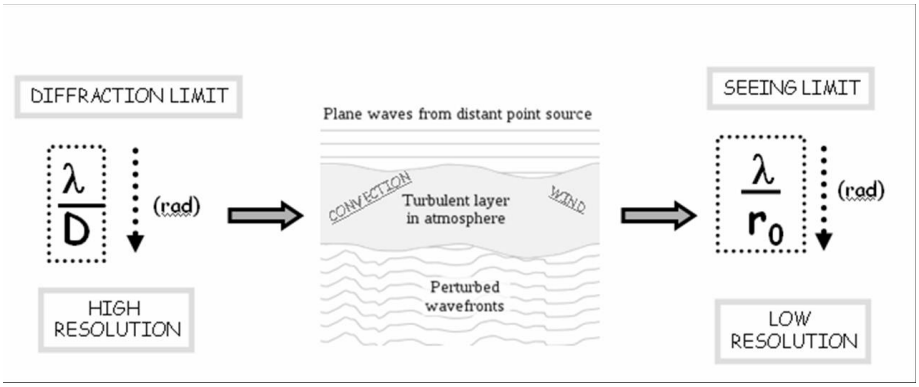

Figure 1.2: Schema of the angular resolution obtained without atmospheric turbulence (on the left), and with atmospheric turbulence (on the right).

An Adaptive Optic (AO) system is able to correct the effect of atmospheric turbulence, and starting from a seeing limited condition (FWHM≅0.5-1.0 arcsec), it is possible to obtain a resolution close to the diffraction limited case (FWHM≅ milliarcsec for a telescope with a diameter of 8m in visible wavelength). Thanks to such a system we are able to use all the potential resolution of the telescope.

The main elements of an AO system are:

- *wavefront corrector*: system (*deformable mirrors*, DM) that can change the shape of the incident wavefront (assuming an equal

but opposite shape).

- *wavefront sensor*, WFS: to sense how the incoming wavefront is distorted.

- *recontructor*: convert the WFS information to DM commands in order for the DM to assume the right shape that compensate the atmospheric distortion.

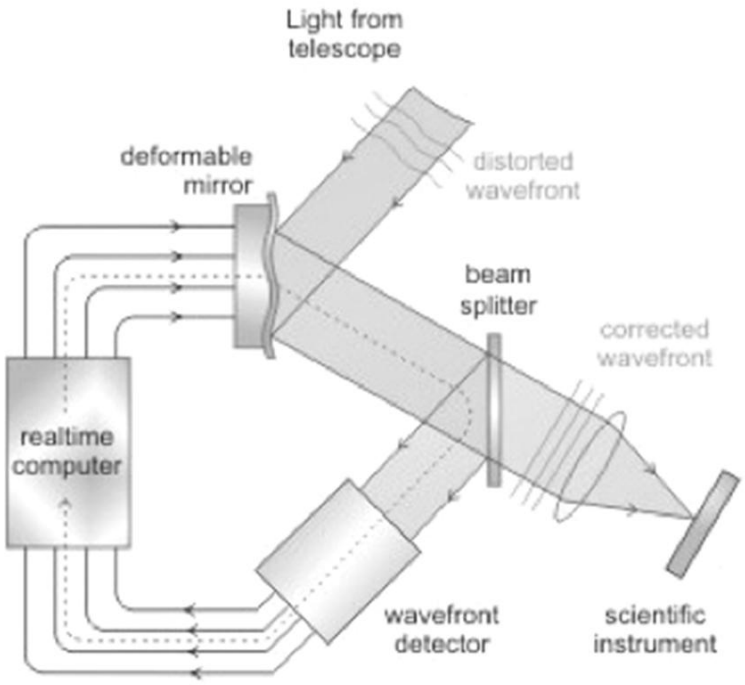

Figure 1.3: The AO main components

In an AO system the controller uses the data measured by the WFS in order to command the mirror actuators with the aim of minimizing the rms residual of the wavefront as best as possible. The correction happens in closed loop: at step *i* the wavefront sensor measures the wavefront residual after the DM correction, starting from these last WFS measures the control system generates the command to give to the corrector for the step *i+1*. The error signal at step *i* is given by:

$$e = s_{ref} - s \tag{1.2}$$

The AO control loop can then be closed around the reference slopes (s_{ref} in the equation 1.2), that are the low-order and static aberrations introduced by the optical components located between the beam splitter and the imaging camera (see figure 1.3, called non common path aberrations). The operation 1.2 changes the mirror shape, and therefore the signals recorded by the wavefront sensor at each iteration. This operation as what we call a *closed loop*.

1.2 The LBT AO system

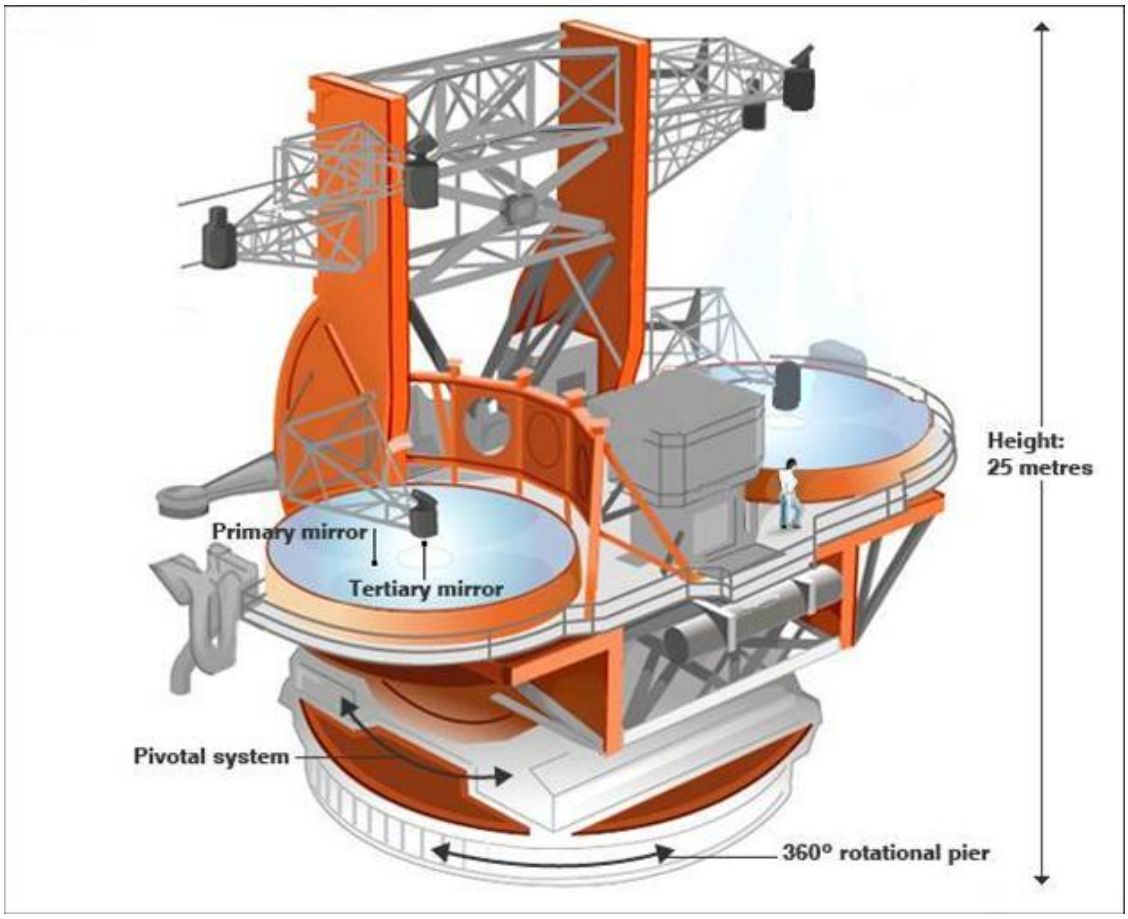

Figure 1.4: The Large Binocular telescope main optical elements: a primary mirror of 8.4m, an adaptive secondary mirror of 0.911m, and a tertiary secondary mirror in order to obtain different Gregorian foci configurations.

The Large Binocular Telescope (LBT,[C.Del Vecchio & al. 2004], [J.Hill & al. 2008]) is a collaboration between institutions in USA, Germany and Italy. The telescope, situated on Mt. Graham in southeastern Arizona, uses two 8.408 meter primary mirrors (PM) to provide a collecting area equivalent to an 11.8 meter circular aperture, it makes the LBT the most powerful single mount telescope in the world in terms of light collection capability. By having both the primary mirrors on the same mounting, the telescope will be able to achieve the diffraction-limited image sharpness of a 22.8 meter aperture. When its two beam-combining interferometers are in routine use, LBT will be the pathfinder for science with the next generation of 20-meter class telescopes, this provides unique capabilities for high resolution imaging of faint objects.
The secondary mirror (SM), concave ellipsoidal mirrors of a Gregorian design) is a secondary deformable mirror (SDM), and thanks to this the adaptive optic system doesn't need any other auxiliary optical system. The SDM has a diameter of 0.911m and its shape is dynamically controlled by 672 magnetic actuators ([A.Riccardi & al. 2004]). The secondary mirrors forms the image at the straight-through Gregorian foci below the primary mirrors. A pair of flat tertiary mirrors can be swung into place to divert the light to Bent Gregorian foci with the permanently mounted large instruments in the very center of the telescope structure (1.5).

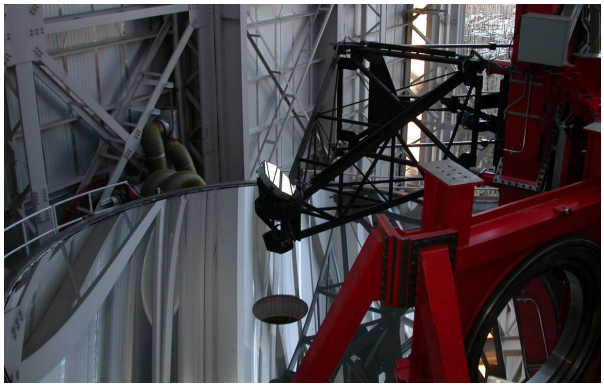

Figure 1.5: This photo shows the tertiary mirror deployed on its swing arm above the left primary mirror of the telescope. In addition to tip-tilt and piston motion, the tertiary can rotate around the optical axis to deliver the F/15 beam to several different focal stations (three with rotators, and two fixed on each side) in the center of the telescope.

The LBT has 10 focal stations to host single-channel and interferometric instruments (see 1.6):

- Below the primary mirrors, two large optical-UV multi-objects double spectrographs (`MODS`) are mounted at the direct Gregorian focal stations.
- Two seeing limited cameras, Large Binocular Cameras (`LBC`), are situated at the f/1.14 prime focus.

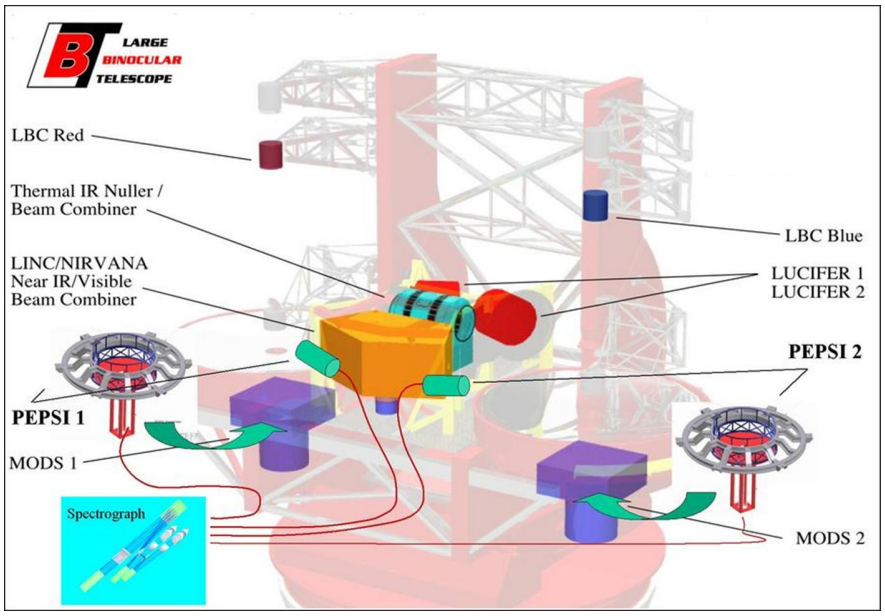

Figure 1.6: The LBT instruments locations

- Two near-IR imagers-spectrographs, `LUCIFER`, for both seeing limited and diffraction limited operations, bended Gregorian focus stations.
- An high-resolution spectrograph with two polarimeters (`PEPSI`) again direct Gregorian focus stations.
- Two interferometers: A mid-IR interferometer (`LBTI`) for nulling interferometry, and a near-IR Fizeau imager,(`LINC-NIRVANA`), are mounted between the two mirrors in order to combine the bended Gregorian beams.

The LBT site

The ForOt group, that works in Astrophysical Observatory of Arcetri (Florence), is studying atmospheric turbulence applied to astronomy. ForOt has studied the astronomical site of Mt.Graham where LBT was built. It has studied the vertical distribution of the optical turbulence (profiles of C_N^2, using the instrument Scidar mounted on Vatican telescope on Mt.Graham not to far from LBT). Reconstructing the C_N^2 profiles is very important because we are able to optimize the adaptive optic instruments that are under integration on the telescope site. In fact this profile is a measure of the turbulence strength as a function of altitude, and it gives a description of the main astronomical parameters at an observatory, like seeing, isoplanatic angle, and coherence time of the wavefront:

$$seeing \approx \frac{\lambda}{r_0}(rad) \tag{1.3}$$

$$r_0 \approx \lambda^{6/5} \cdot \left(\int C_N^2(h) dh \right)^{-3/5} \tag{1.4}$$

$$\vartheta_0 \approx \frac{r_0}{H} \tag{1.5}$$

(H:altitude of the turbulence layer i.e 10Km)

$$\tau_0 \approx \frac{r_0}{V_{wind}} \tag{1.6}$$

(V_{wind} is the wind velocity i.e $10 ms^{-1}$)

From the previous equations (1.3,1.4,1.5,1.6) we understand the importance of the measure of C_N^2 profiles in order to characterize the adaptive optic main components of LBT a Mt.Graham ([E.Masciadri & al. 2010]).

From the measure in table (1.7) we can deduce that Mt.Graham is an excellent site for the turbulence effects, it can be comparable to the best sites of the world, like Mauna Kea (Hawaii)

1.3 The giant telescopes era (E-ELTs)

There are actually a class of infrared(IR)/optical telescopes of large diameter. At first Keck I and Keck II (started the operations 1993, 1996 respectively, on

Parameters	ε	θ_0	τ_0
Units	(")	(")	(msec)
Mt. Graham(*)	0.72	2.50	4.8
Mauna Kea(**)	0.79	2.69	5.1

(*) Generalized Scidar (**) DIMM at h=6.5 m

Figure 1.7: The main astroclimatic parameters evaluated at Mt.Graham ([E.Masciadri & al. 2010]) and at Mauna kea site ([M.Schoeck & al. 2009]): ϵ is the medium value of seeing (arcsec), ϑ_0 is the isoplanatic angle,τ_0 is the time coherence of the wavefront.

the summit of Mauna Kea in Hawai'i) with their 10m primary mirror (PM); the 4 UTs at Very Large Telescope of 8.2m PM each one (the first UT started the operations in 1999, on Cerro Paranal, Chile); the two Gemini telescopes of 8m PM (started the operations 1999 for both, Gemini North on Mauna Kea in Hawaii, Gemini South on Cerro Pachón, Ande, Cile); Subaru of 8,2m of PM (started the operations 2000,on Mauna Kea in Hawaii). The most recent telescope of 8m class is LBT, and soon the Gran Telescope of Canarias (10.4m of primary mirror, Roque de los Muchachos Observatory on the island of La Palma) will be operating.

The projects for the next generation of IR/optical telescopes are characterized by very large diameters, in fact they are called Extremely Large Telescopes (***ELT***s), with a primary mirror more than 20m of diameter. There were several telescopes in various stages of design or construction until 2000, but only three developed into construction projects:

- The Giant Magellan Telescope (`GMT`) is a ground-based telescope planned for completion in 2018. It will consist of seven 8.4 m diameter primary segments, in a Gregorian configuration, forming a collecting area equivalent to 21.4 m one. A characteristic is that the secondary mirror is composed by seven thin adaptive shells (total dimension of about 3m), each one mapping to a single PM shell (see figure 1.8).

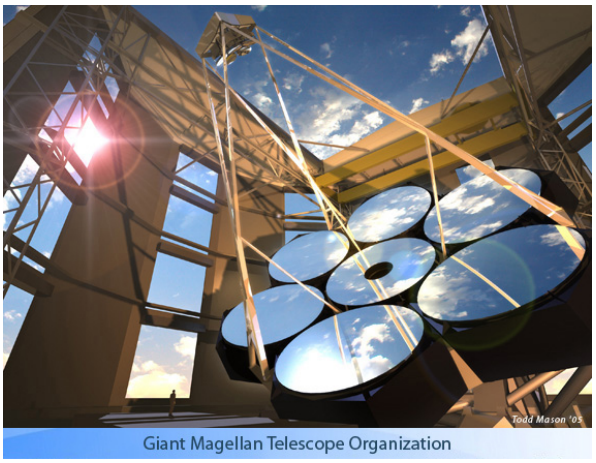

Figure 1.8: A design of the GMT: the primary segmented mirror is composed by 7 segments, and the secondary one is also composed by composed by seven segments.

- The Thirty Meter Telescope (`TMT`) has a Ritchey-Chrétien configuration, with a 30 meter diameter primary mirror, that will be segmented into 492 smaller (1.4 m) individual hexagonal mirrors, and an active secondary mirror. The tertiary mirror is used to fold and steer the light path so that the science beam can be delivered to any of eight instruments that will be mounted on the two main Nasmyth platforms (see figure 1.9).

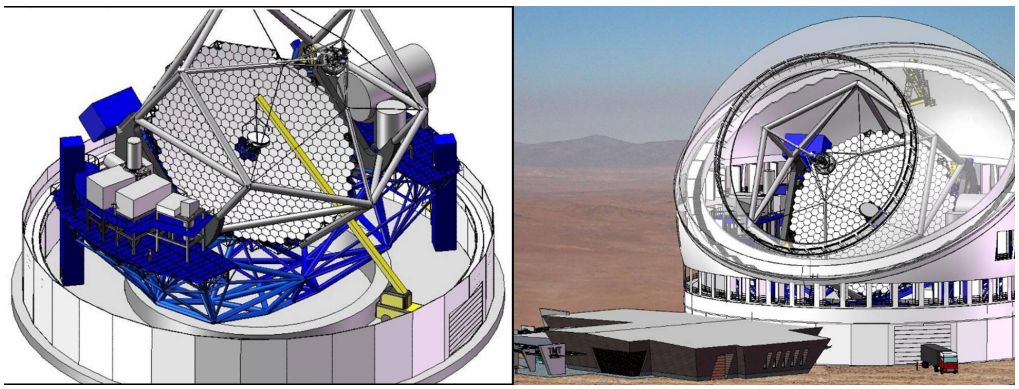

Figure 1.9: A design of the TMT: primary mirror of 30m, secondary active mirror and a tertiary mirror. On the right a design of the dome that hosts the telescope.

- The European Extremely Large Telescope (`E-ELT`) is an extremely large telescope design composed by five mirrors, and proposed for the next-generation European Southern Observatory optical

telescope. The primary mirror has a diameter aperture of 42m, it will be composed of about 984 hexagonal segments, about 1.4m wide and 5cm thick. The optical design calls for an immense secondary mirror 6m in diameter. The construction period is estimated to be 5-6 years leading to first light around 2016. A tertiary mirror, 4.2 m in diameter, relays the light to the adaptive optics system, which is composed of two mirrors: a 2.5m mirror supported by 5000 or more actuators so as to be able to distort its own shape a thousand times per second, and one 2.7 m in diameter that allows for the final image corrections (see figure 1.10).

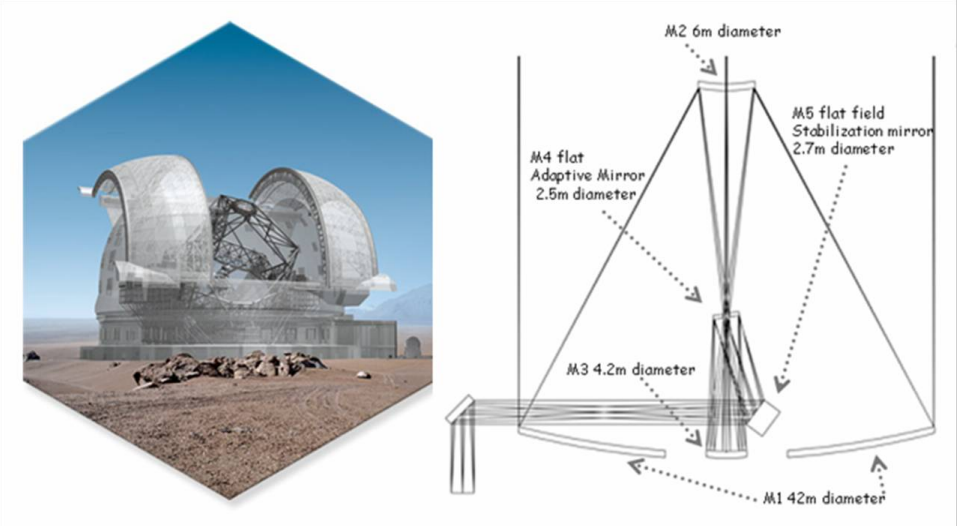

Figure 1.10: on the right the dome project for the EELT, on the left a schema of the main optical components.

Now we want to understand which position LBT has in this background. We can say that LBT is a 'forefront telescope' for the 8-10m class because of its secondary adaptive mirror in place of the conventional one: this approach has unique advantages in terms of optical simplicity, high throughput and low emissivity (see figure 1.11).

At the same time the LBT is also an example for ELT, because of the hight order adaptive mirror that will also have (see figure 1.12).

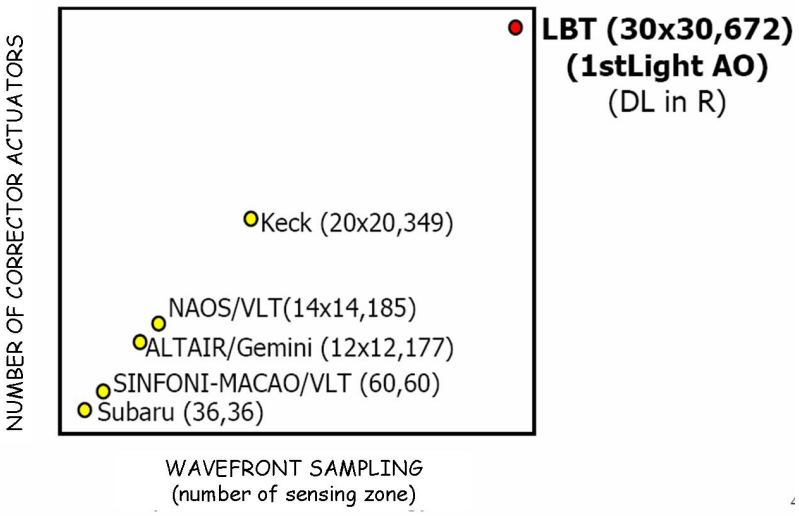

Figure 1.11: A comparison of LBT with existing astronomical single-conjugate system of class 8-10m of telescope

Name	Image	aperture (m)	Equiv. ap. area	Area (m^2)	M1 Mirror	Note
European Extremely Large Telescope (E-ELT) Image credit ESO		42	42	1300 m^2	984 × 1.45 m hexagonal segments (*f*/1)	Largest with funding
Thirty Meter Telescope (TMT)		30	30	655 m^2	492 × 1.45 hexagonal segments (*f*/1)	Site Chosen
Giant Magellan Telescope (GMT)		24.5	21.4	368 m^2	7 × 8.4 m mirrors	Site chosen, 1 mirror cast
Large Binocular Telescope (LBT)		22.8	11.7	111 m^2	2 × 8.4 m M1 mirrors; 1 mount (2 × M1)	Largest Binocular; largest non-segmented mirrors; Fully operational 2008

Figure 1.12: A comparison between LBT and ELT.

In order to do this, ELTs need a lot of actuators in order to correct the atmospheric aberration effects. In fact the number of independent actuators that are required for a telescope of diameter equal to D, is (equation 1.7):

$$N_{actuators} \cong \left(\frac{D}{r_0}\right)^2 \tag{1.7}$$

So we can understand why the new generation of 20m class needs a haigh number of actuators. Remembering that the configuration of the independent actuators is determined by the WFS sampling, so that the WFS is able to estimate the wavefront perturbations in a number of points equal to the number of actuators. Therefore, the WFS needs a number of sensing zones with a dimension on the pupil equal to r_0 (see the number of actuators and sensing zone for LBT case on the figure 1.11).

Chapter 2

Set up of the whole AO system

2.1 The adaptive optic system at the telescope

The Adaptive Optic system to be used in LBT, except the secondary DM, is part of Acquisition, Guiding and Wavefront (AGW) sensing unit mounted inside the system derotator in front of the telescope bent Gregorian foci. This unit contains all the AO system opto-mechanics and electronics.
The instrument coupled with the AO system is called LUCIFER ([H.Mandel & al.2001]): a NIR instrument which aim is imaging and spectroscopy of very faint point sources, that works in mode seeing and diffraction limited imaging, in a wavelength range of 0.9-2.5 μ, with a resolution of 5000-10000 (seeing limited)and 21000-37000 (diffraction limited), and with a FOV of 4 x 4 arcmin (seeing limited), 0.5 x 0.5 arcmin (diffraction limited).

The main components of the LBT AO system are (see figure 2.1):

- A deformable secondary mirror with a diameter of 911mm and composed by a thin (1.5-2.0mm) deformable shell controlled in position with large-stroke (about 0.1mm) electromagnetic (voice-coil like) force actuators (672) and using internal capacitive sensors as position feedback.
- A pyramid wavefront sensor with tree main pupils sampling: the maximum one is 30x30 subapertures, the others two are 20x20 and 10x10. We can choose between these configurations with no change in the optical configuration system, but simply modifing the binning value of the CCD.

- A control system that reconstructs the wavefront and send the commands to the DM in order to correct it.

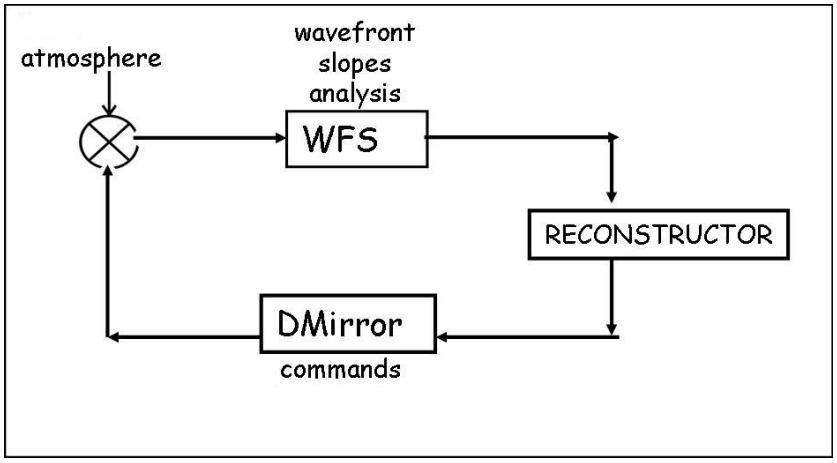

Figure 2.1: A short schema of the main components of AO loop: the detector of the wavefront errors (sensor), the corrector of the wavefront errors (DM), the element that links this two parts (reconstructor).

2.2 The deformable secondary mirror

The two adaptive secondary (AS) mirrors for LBT with their 672 actuators represent the new generation of the AS technology. Their design is based on the experience earned during the extensive tests of the previous generation units, especially on the 336-actuator AS mirror for the 6.5m conversion of the MMT
([S. C. West & al. 2002]), but both the optical manufacturing procedure and the electro-mechanics design have been revised, improving performances, stability, reliability, maintenance and the computational power of the system ([A.Riccardi & al. Feb. 2003],[A.Riccardi & al. Dec. 2003]). The Large Binocular Telescope has two instruments that rely on adaptive optics secondary mirrors as wave-front correctors of the atmospheric turbulence and wind-shaking effects: one is the first-light system, that will provide two units for independent single-conjugate correction for each 8.4m primary mirror, LUCIFER. The other is an interferometric multi-conjugate AO system called NIRVANA (see figure 1.6 in chapter one).

The possibility to use the secondary mirror as deformable mirror (DM) for an AO system has several advantages, especially in our practical implementation with electromagnetic force actuators and capacitive position sensors ([P.Salinari & al. 1993]):

- The deformable mirror is used like a secondary one, so it avoids the introduction of relay optics, simplifing the system and reducing the problem of extra warm reflections in the infrared.
- The same DM can serve all the focal stations of the telescope.
- The large stroke of actuators (≈1mm) is able to obtain both high order and low order correction.
- The electromagnetic actuators are capacitive type and do not suffer from hysteresis.
- The electromagnetic actuators do not have any physical contact with the deformable shell, simplifying the replacement of a dead actuator.

2.2.1 The linear model of the secondary deformable mirror

We can have situations that give rise to non-linearity response of the SDM. It happens for saturation behavior due to a limited force range with which the actuators can be moved. This risk is increasing when the atmospheric condition is worse, in fact this corresponds to a bigger fluctuation phase to be corrected. Inside the right force range to be applied to actuators, we can consider the mirror as linear in behavior, and so we can express the phase correction as linear combination of *influence functions*(IF) indicated by U(r): the $\mathrm{U(r)}_j$-one represents the deformation obtained when a unit of signal control is applied to the j-actuator (the other j-1 actuators are keeping still). We can write for a number of actuators equal to n_{act}:

$$\varphi_{cor}(r,t) = \sum_{n_act}^{i=1} u_i(t) U_i(r) \tag{2.1}$$

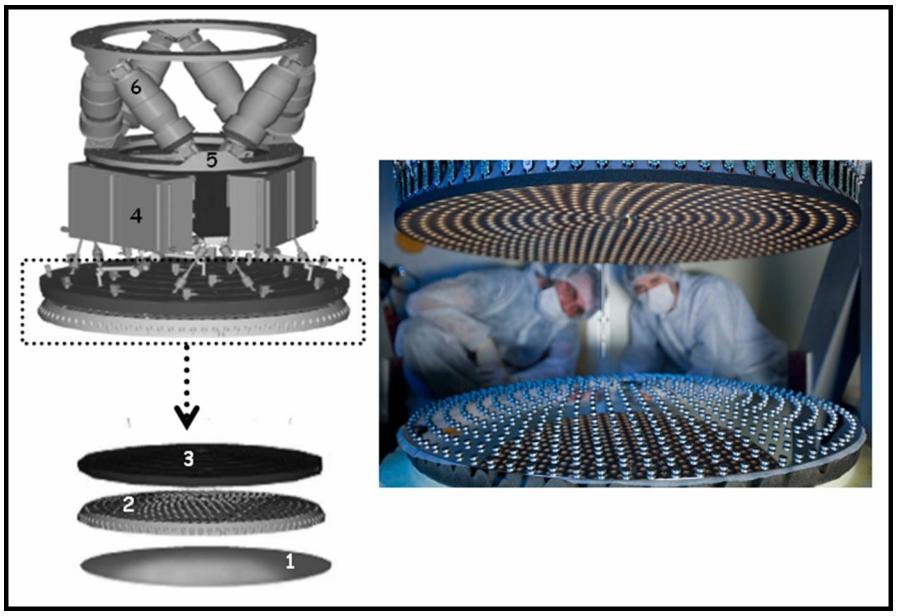

Figure 2.2: On the left schema of main components of secondary deformable mirror: 1)1.6mm thick deformable shell;2) 50mm thick Zerodur reference-plate;3) cold plate and actuators support;4) 3 cooled electronic boxes;5) interface frange and structural support;6) Hexapod. On the right a picture of the shell.

In the equation 2.1 the $u_i(t)$ is the coefficient of signal control applied to the i-th actuator, and after the SDM correction the residual phase can be writeten as:

$$\varphi_{res}(r,t) = \varphi_{turb}(r,t) - \varphi_{cor}(r,t) \tag{2.2}$$

In equation 2.2 the φ_{res} is the residual phase after DM correction and the φ_{turb} is the turbolence phase at the same instant t. We can express the equation 2.1 in matrix form if we decompose each influence function on a $n_{pix} \cdot n_{pix}$, so N is the *influence matrix* where each column is a vector $U_i(k)$ by n^2_{pix} dimensions, where $k=[1,...,n^2_{pix}]$. We can re-write the column vector u(t) containing the coefficient of signal control, and the vector φ_{cor}, we obtain:

$$\varphi_{res}(k,t) = Nu(t) \tag{2.3}$$

We can also express the influence function by the mirror base: if the IFs are independent, they form a base of the mirror space with a dimension equal to the number of actuators. By this base the control signals u ($[u_1,...,u_{nact}]$ are the modal coordinates and the IFs are the mirror modes. So we are able to

express the phase mirror corrector also by the mirror modes and not only by polynomial Zernike modes or Karhunen-Loeve modes.

2.3 The AGW unit

The AGW units will be mounted at LBT in front of the Gregorian focus where a cylindrical volume with a diameter of 1390 mm and a length of 470 mm is available. This volume is the same for all the bent Gregorian foci[J.Storm & al.2000]. The AGW has been realized at AIP. while the WFS at Arcetri Observatory [S.Esposito & al.2006]. It is composed by two parts: an off-axis system for target acquisition, guiding and slow wavefront sensing, and the on-axis system for wavefront sensor correction. The off-axis component is able to control the AGW in order to maintain the optimum setting of the optical system during observations. The on-axis system operates on the optical light reflected off by a tilted entrance window for the instrument science camera: Lucifer. In this way both the correction to the wavefront (done with the secondary mirrors) and the wavefront sensing (done on the light reflected off the dewar entrance windows) is performed without introducing a single additional optical surface in the science beam [J.Storm & al.2000].

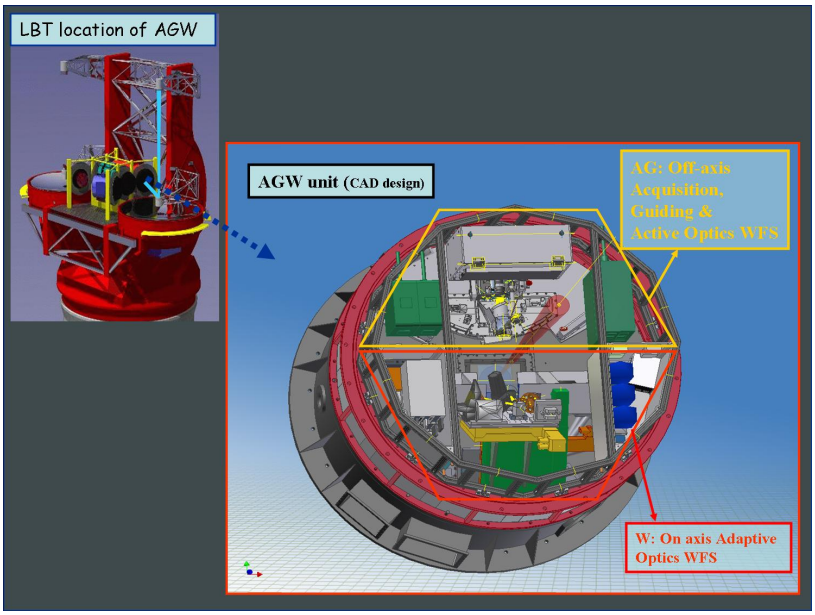

Figure 2.3: left:a 3d CAD drawing of the AGW location at LBT telescope.On the right the AGE two principal components: the off-axis system and the on-axis system.

The main component of on-axis AGW are:

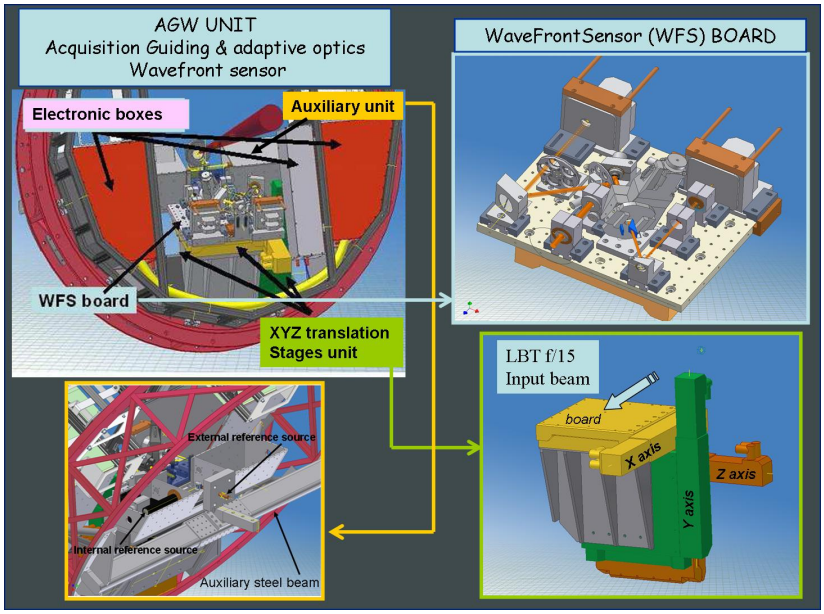

Figure 2.4: The whole AGW 3d drawing, and the principal components of on-axis AGW:

- *The translation stages assembly.* Two of these tree stages (X,Y) are able to translate the WFS unit in the f/15 focal plane of the LBT Gregorian focus, in order to acquire the reference source. The third one (Z) is moving the WFS unit in order to focus it. Optical encoders placed on the stages themselves are used to control the stages positioning [S.Esposito & al.2006].

- *The unit electronic boxes.* The two principal boxes are collocated in the side parts of the WFS board, they are covered by 20mm of styrodur, in order to satisfy the LBT requirements, about the thermal uniformity. This thermal isolation is needed to prevent some temperature gradient formation, that is able to generate turbulence inside the optical path. In the main time they need also a thermal stability of all the electronic components inside, particularly of the CCD controllers. For these reasons there is a hydraulic cooling system that is able to keep the box temperatures below 25°C by a flux of 4-5 l/mm of glycol and water at 3°C below the ambient temperature.

- *The auxiliary unit bench.* It contains mainly the WFS reference fiber. The LBT light source is an optical system that generates an f/14.5 beam having an imaginary pupil of 945 mm diameter at 13665 mm as the real one that coincide with the secondary DM. Some preliminary laboratory measurements have been realized in order to characterize the system in terms of PSF and pupil quality. An optical fiber from an halogen wideband source lamp feeds a small optical system that illuminates the wavefront sensor board [A.Tozzi 2003].

- *The wavefront sensor board.*The NGS wavefront sensing unit is realized using very small and standard optical elements. This is possible because the secondary deformable mirror is used as a pupil stop of LBT [D.Gallieni & al.2003],[A.Riccardi & al.2004], so that we do not have to conjugate the telescope pupil to the DM in the optical train of the WFS, and thanks to the adoption of a movable WFS board using the three translation stages, they are able to achieve the field of view of 3x2 arcmin for reference star acquisition. The dimension of the board are 320x400mm, and it has two sensing channels: one for the pyramid wavefront sensor proposed by R.Ragazzoni [R.Ragazzoni.1996], where optical components are optimized for that wavelength range of 600nm-950nm, with a WFS optical train length of 500mm; the other channel is providing an f/45 focal plane for AO system closed loop operation test and for star acquisition during telescope observation.

2.3.1 The main components of WFS board

The on-axis system operates on the optical light reflected by a tilted dichroic surface that lets the near-IR light pass through to the instrument science camera, and reflects the optical light back to the wavefront sensing system. This entrance window for the WFS called the Lucifer Window, is placed 123mm above the nominal focus and is tilted by 15°.

In figure 2.5 WFS board is shown with all the main components. A description of them is in the following. The light analyzed by the WFS is reflected

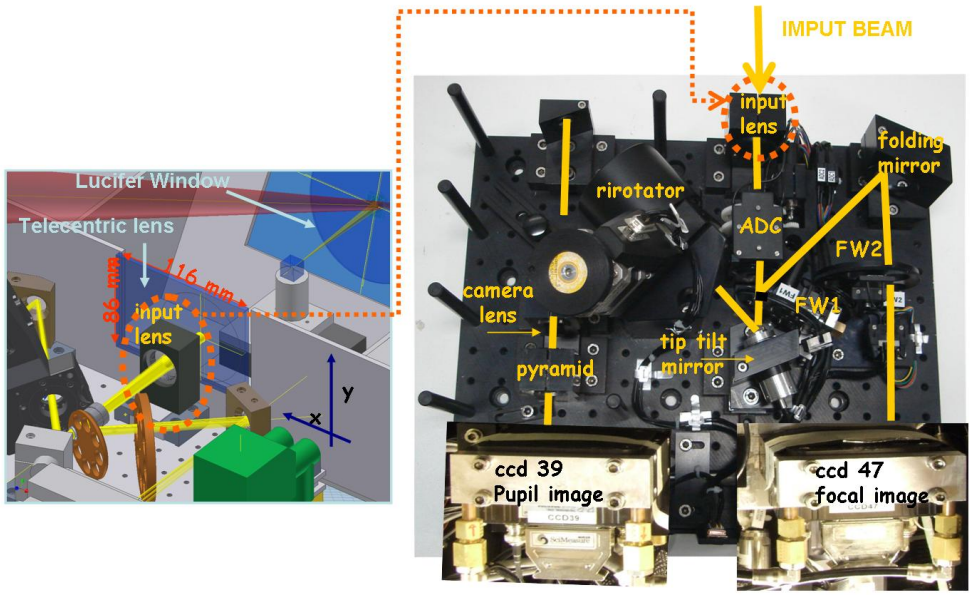

Figure 2.5: In the corner on the upper left: a 3d drawing of the input window of the AGW, Lucifer Window. The telecentric lens is also indicated, from its center it has an exploring area of 3x2 FOV in arcmin.

off by the Lucifer window, and goes through a telecentric lens (that is able to obtain parallel beams for different incoming fields), and after about 30mm it meets with the first optical board element: the *input lens L1*. It's a refocusing triplet that provides an f/45 focused on the vertex of the pyramid. After L1 we find an Atmospheric Dispersion Corrector (*ADC*): it's the device that compensates the effect of differential atmospheric refraction (a consequence of the wavelength-dependent index of refraction of the atmosphere); the light passes trough a filter wheel (*FW1*): it has five different filters for the different Adaptive Optics configurations. The windows are used to split the incoming F/45 telescope beam into the technical viewer branch for CCD47 acquisition camera for the pupil image, and the wavefront sensor branch for the CCD39 acquisition camera for the focal image. Now the description is split into two optical path branches, in order to simplify it.

In the technical viewer branch, the light coming from FW1 goes through a *folding mirror*, that send it through another filter wheel (*FW2*). The light is now analyzed by the acquisition camera, a Marconi *CCD47* BI with 7.2"x7.2" of FOV. In the wavefront sensor branch, the light coming from FW1 is reflected

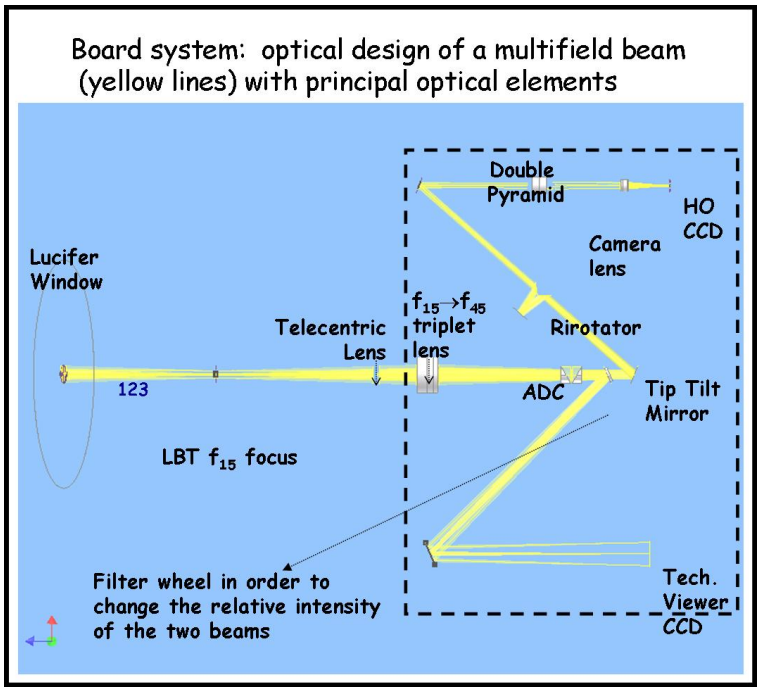

Figure 2.6: An optical scheme of the board set-up. In blue the distance between optical elements in mm.

by a mirror mounted on a piezo-driven fast steering stage (*Tip-Tilt mirror*,or TT mirror). L1 input lens refocus the pupil image of the telescope (the adaptive secondary) 27mm before this TT mirror (see figure 2.6), that provides the tilt modulation needed to operate the pyramid sensor. It's able to modulate in a range of $\pm$ 0.8 arcsec. The beam coming from the TT goes through the *Rerotator* (three reflecting mirror mounted on a commercial rotational stage): it is necessary to contro-rotate the apparent rotation of the secondary DM 672 actuators on the CCD39. This because the AGW is de-rotated while the SDM is keeping still respect to it. The F/45 beam outgoing from the RR is folded by a mirror and focused on the pyramid. It's the main optical component of the board, it's collocated on the F/45 focal plane. The pyramid design is made in Arcetri[A.Tozzi & al.2008], and it's a double pyramid instead of a single one, for two main reasons: the first it is that is possible to have pyramids with a base angle greater then the one of a single pyramid, so it's possible to obtain a better optical accuracy on the edges ; the second reason is the possibility to choose a pair of glasses that are able to reduce the chromatic effect [A.Tozzi & al.2008]. After the focusing of the beam on its vertex, the

Pyramid sensor separates the beam into 4 parts and pass through a camera lens of focal length 35mm, that realizes 4 pupils image of SDM on the CCD39 viewer.

All these elements need of an accurate procedure in order to be optically alligned. In this phd work's thesis there is a contribution to this alignment procedure of some components. The following chapters report on the main steps of these contributions for each one of these elements: the atmospheric dispersion corrector, the Rerotator element, and the phase screen, although, at the end, this last component has not been used, because a better solution has been found in order to simulate an atmospheric disturbance, as it will be explained in the following.

2.3.2 The *A*tmospheric *D*ispertion *C*orrector (ADC)

In the case of a natural reference star an ADC can improve the image quality on the wavefront sensor and consequently improve the sensitivity of the system. In fact the wavelength-dependent index of refraction of the atmosphere generates some dispersion of the light. The importance of atmospheric dispersion increases rapidly with increasing zenith angle and decreasing wavelength, and so infrared observations (more than 0.8μm) are rarely affected [A.Filippenko 1982], while in the visible wavelength range this contribution is not negligible (it's the work wavelength range of AGW AO system).
There is a main requirement for an ADC : a variable dispersion to compensate one introduced by the atmosphere at a given zenith angle. For LBT the ADC is able to compensate for the atmospheric dispersion between 0° to 70°, having a diffraction limited PSF in the wavefront sensor focal plane. This is to maintain the smallest PSF possible and so to use the pyramid sensor at the maximum sensitivity. The diffraction limited PSF for the WFS central wavelength at 0.75μm has a radius of 11.25μm so the chromatic dispersion has to be negligible with respect to this. This requirement suggests counter rotating prisms with dispersion a maximum (minimum) when the apex angles of the prisms are in the same (opposite) directions.
With an ideal ADC the image of a star shows no dispersion at Zenith angle, as

well as no large displacement from a nominal position on the detector. Thus there are two basic requirements for an ADC:

- variable dispersion to compensate that of the atmosphere at given zenith angle
- Zero-deviation at some mean wavelength, within the range of interest for all zenith angle.

The selection of the individual prism angles depends on the telescope and configuration in which the ADC is used. The ADC for LBT AGW unit is composed by two couples of prisms with a diameter of about 12 mm and a thickness of about 4.5 mm. They are assembled inside a mechanical mount that is able to move one couple with each other using two motor .

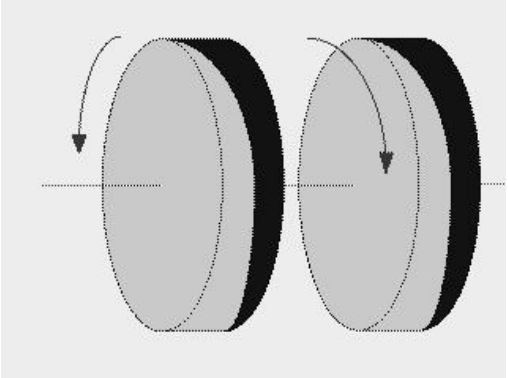

Figure 2.7: A simple design of the two couple of controrotating prisms.

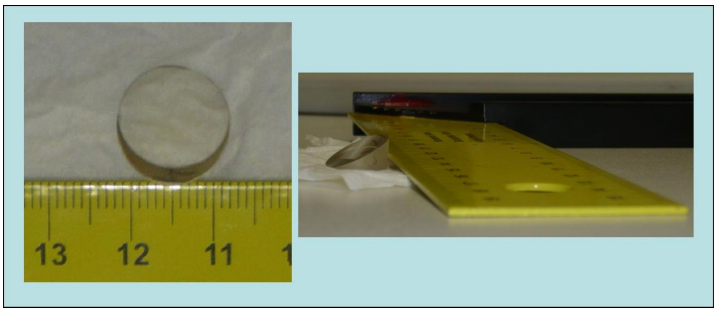

Figure 2.8: A picture of a real glass component of a couple of prisms: diameter of about 12 mm and a thickness of about 4.5 mm. the glass type is C04-64, with index nd=1.603.

ADC description

An ADC can consist essentially of an Amici prism system. The simplest form of an Amici prism system consists of a cemented double of two prisms, one being of higher dispersion glass then the other, and the prism angle being chosen so that a collimated light beam on traversing the prisms emerges parallel to the incident beam. Usually the beam will be displaced sideways, but it will remain collimated. Collimated beams of longer or shorter wavelengths will be dispersed in opposite directions, and differently displaced, but they will remain collimated. There is a wavelength, for each couple of prisms, where the refraction indexes of the two glasses assume the same value, and this condition is called of the 'zero-deviation' ([C.G Wynne 1997]) this wavelength is called the 'mean wavelength'. The light of the mean wavelength is undeviated, while longer and shorter wavelengths are deviated (it's related to each single couple of prisms composed the ADC).
Each of Amici prism system produces dispersion, over the required wavelength range around the mean wavelength, which value is half of the atmospheric dispersion at the maximum zenith angle to be corrected. At smaller zenith angles, the two separate doublet prism couples are rotated in opposite directions to reduce dispersion (these two prisms have to be mounted so that each can be rotated about the optical axis of the telescope). So the two doublets must be free to rotate independently: when they are in opposite orientations they would give theoretically a null dispersion, while they give the maximum one when their orientation is the same.
The two couples of the ADC's prisms are composed of two glass types (C04-64 and BAM23).In the next figure there is the mechanical design of the ADC support, we are able to move the two couples of prisms controlling the position angle of two motors: we choise the angle for each wheel that moves the single couple. The accuracy of rotation angle is of the order of hundredth of degree.

Tests of the ADC dispersion

In order to evaluate the behavior of ADC correction, we use a Zemax simulation of the whole LBT board optical system, setting all the parameters of

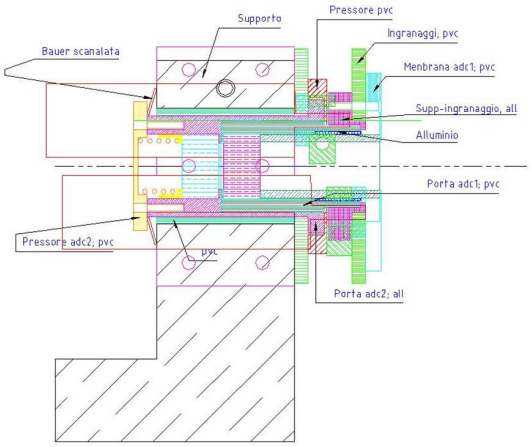

Figure 2.9: The mechanical support of ADC, realized in Arcetri

the two couple of prisms (apex angles, refraction index, etc). By this simulation we can evaluate both the behavior and the possible sources of errors. In the laboratory tests we are not able to check the right behavior of the ADC for each Zenith angle, but we have tested the displacements for some wavelength at zero zenith angle; we have compared the laboratory measures with the Zemax results, by measuring the residual correction at different wavelength (in a range between 650nm to 900nm). We have noticed a discrepancy, and a solution has been found putting this error to the wrong nominal value of the refraction indexes of the prisms. In fact putting the right values inside the simulations we found the correspondence between the real and simulated results, see figure 2.10.

Obviously we can check this only the for zero zenith angle. In order to evaluate the residual dispersion at all zenith angle (from 0° to 70°) we can use only simulations, for each zenith angle we found an ADC contro-rotating angle of correction and we check about the residual dispersion values for each wavelength (in the range between 0.600-0.950 micron). Atmospheric dispersion and residual values for each angle are plotted in figure 2.11, and we can see that it has be found a maximum PSF dispersion value of 10 micron for a zenith angle of 70° (on image plane f/45), that is negligible respect to the diffraction limited PSF (41μm at 0.75μm).

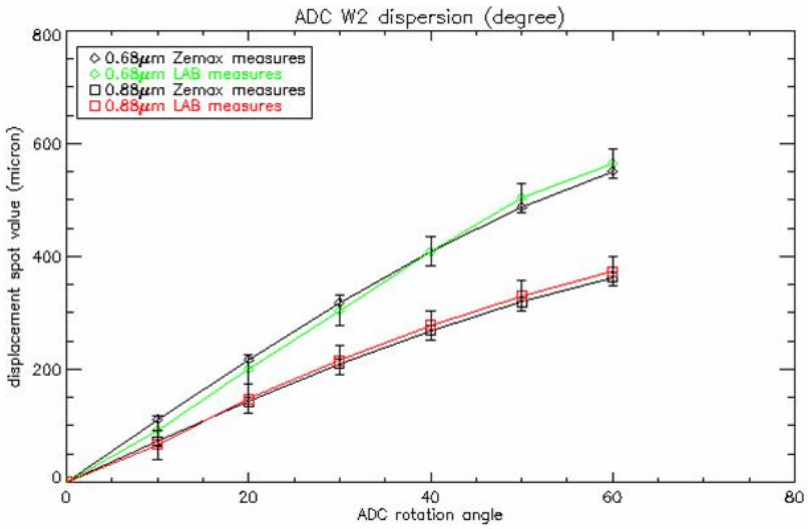

Figure 2.10: red,green: the displacement values (micron) for each ADC rotating angle at 0° zenith angle of laboratory measures at 680nm, 880 nm respectively; black: the Zemax simulation results in the same condition.

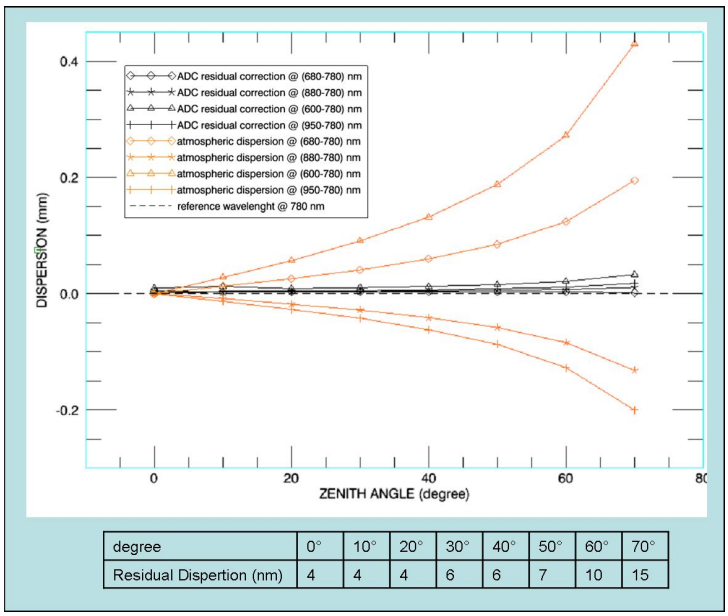

degree	0°	10°	20°	30°	40°	50°	60°	70°
Residual Dispertion (nm)	4	4	4	6	6	7	10	15

Figure 2.11: Orange line: the atmospheric dispersion, for zenith between 0° and 70° by step of 10°. Black line: residual in nm after the ADC correction at the wavelength selected and for each angle; this is the maximum residual dispersion between the wavelength range measured on image plane f/45. The wavelength at 780 nm is the reference, it's the zero-deviated one.

2.3.3 The Rerotator (RR)

The WFS is located into the AGW derotator that corrects the apparent sky rotation, instead the DM is keeping still respect to it, and so, in order to keep

the same correspondence between M2 actuators and pixel pupil image, the footprint of the 672 actuators has to be correct using another pupil Rerotator [A.Tozzi & al. 2003], located on the AGW board. The f/45 focal image is necessarily located at the vertex of the pyramid sensor during integration time, and we are able to guarantee it thanks to the centering of X,Y stages. Also the PSF image has to be showed with the technical viewer (on the focal plane), but it is a less restricted constrain respect pyramid one, in fact thanks to X,Y stage we are able to center the PSF moving the whole board.

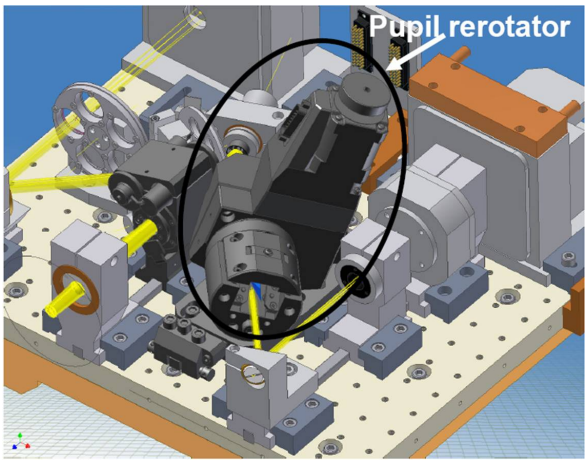

Figure 2.12: The rerotator assembled on the optical board

Optical description and behaviour of the RR

The rerotar is composed by tree reflecting mirrors: one flat mirror, and a 120° couple mirrors. The rotation of these allows us to guarantee a bijection between the DM 672 actuators and the pixel pupil image on CCD39.

Only one well-work configuration exists: the output beam from the last RR mirror is parallel to the input one into the RR system. Obviously it's necessary to align it as better as possible in order to obtain this best configuration, and we can defined it as a function of the parameters characterized RR (the altitude of the reflecting prisms,the distance of the vertex of this prism respect to the flat mirror). The rotator misalignments have two components, and we are able to distinguish them thanks to the different consequences generated on the pupil image and PSF displacement:

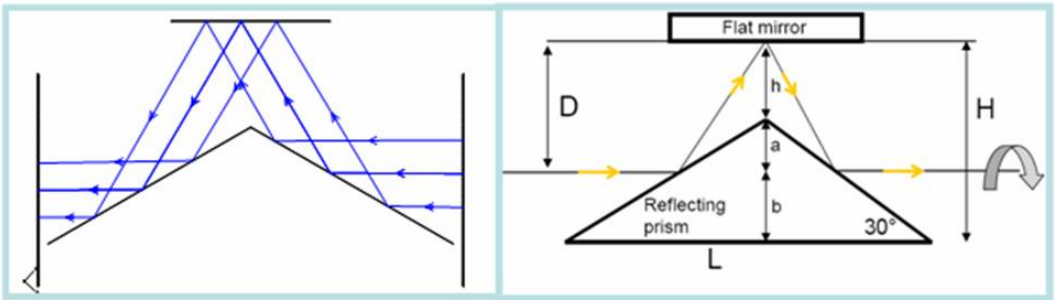

Figure 2.13: left: a Zemax optical design of the RR optical components. Right: a design of the beam reflected on the tree RR morrors in the well-work configuration; the output beam direction is aligned with the input

- An internal misalignment occurs when one of the internal optics gets out of alignment, respect to the well-aligned configuration.The internal misalignment induces a circular displacement of the pupil and PSF whose period is the same as the rotator period.

- An external misalignment occurs when the rotator, as a whole, gets out of alignment starting from this same well-aligned configuration, or, equivalently, when the input beam is modified respect to the optical axis of the rotator. For example, in the image plane, this is equivalent to a displacement of the PSF around the rotator axis. Same thing for the pupil image on the CCD39. The external misalignment induces a circular displacement of pupil and image whose period is half the rotator period.

The two kinds of misalignments have been dealt in laboratory as well as using optical simulation, that are able to reproduce the laboratory behaviors. The internal misalignment has been measured by laboratory tests. The main alignment steps are to measure the distance for the four main positions of RR: 0°, 90°, 180°, 270°, of the PSF and pupil image. In fact the position at 0° and 180° give us information about Y displacement, while the position of 90° and 270° give us information about the X displacement ;the 0°,180°(90°,270°) rotation of the tree mirrors has the same y(x) coordinate. These four position have been measured at four different distances: 30mm,200mm,3.2m,28m, and the two last distances allow us to distinguish the tilt contribute that is preponderant with respect to the decenter that are been caused by the RR

internal mirrors. So the analysis of the difference position between 0°-180° and 90°-270° gives us information about y and x displacement respectively. The main results derived from these measures, in fact using them it's possible to estimate the pupil and PSF displacement for 360° of RR angle in the W board, as it reported in the table 2.14.

Measurement	Requirement	Estimated result
PSF total displacement	0.5 arcsec 0.9mm	0.2 arcsec 0.360mm
PSF displacement during integration	9 um (2.5 deg rotation)	8 um (2.5 deg rotation)
Pupil image total center displacement	+/- 2 pix	+/-0.3 pix
Pupil image displacement during integration	0.1 pix (2.5 deg rotation)	+/- 0.02 pix

Figure 2.14: The pupil and PSF displacement for 360° of RR angle in the W board

Thanks to some simulations it has been possible to introduce the decenter and tilt evaluated by laboratory measurements, and check at the same distances as laboratory, the displacements resulting. The measures seem to be in good agreement each other.

The external misalignment has been measured putting the RR on the WFS board and using an auxiliary CCD on the F/45 PSF using a pellicle beam splitter in order to register the image displacement during RR movement; at the same time we have registered the Pupil position on the pupil-image camera (CCD39). At the same time we are able to save the frames on these two CCD, analyzing them (with a specific procedure) it's possible to obtain the displcementes of the center of PSF and Pupil recorded. From this type of graph we are able to have information about the external misalignment and to correct it (see also table 2.14).

2.3.4 The simulation of atmospheric turbulence

We need a turbulence simulator during Arcetri tests of AGW and secondary DM AO-system, in order to obtain an environment similar to the telescope one. It is necessary to give a brief introduction: the first idea about simulating

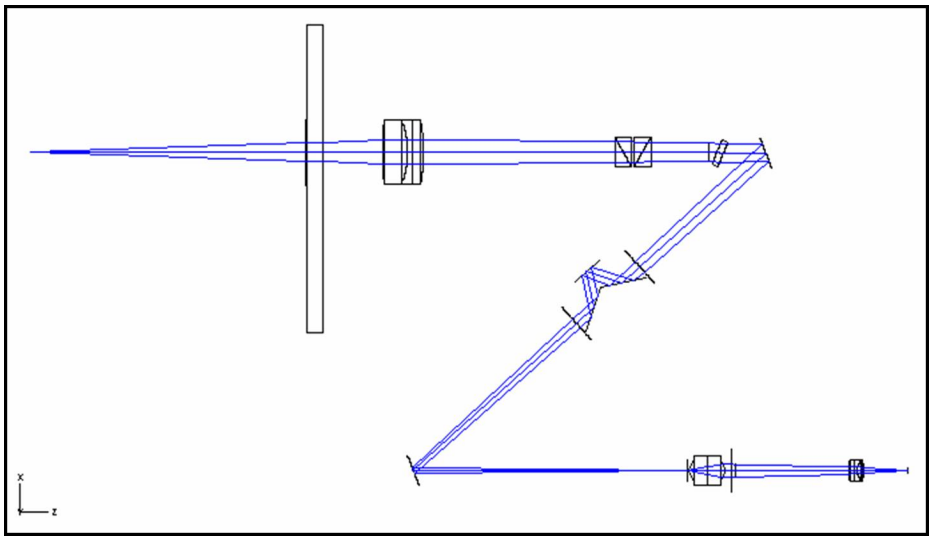

Figure 2.15: A Zemax design of the optical component used in order to measure the external misalignment on the board. There are only two component added to the WFS optical set-up: the auxiliary beam splitter and the auxiliary ccd, in order to measure the PSF simultaneously to the pupil measure on the ccd39.

Measurement	Requirement	Result
Pupil image total center displacement	+/- 2 pix[4]	+/- 0.6 pix
Pupil image displacement during integration	0.1 pix (2.5° rotation)	90°: 0.05 px 180°: 0.05 px 270°: 0.05 px 360°: 0.05 px

Figure 2.16: The following residual misalignment has been found out. The values are compatible with the estimated ones, as we can see in the table.

the atmospheric turbulence was to make use of a phase screen. Later it was replaced by a software, that is able to simulate the atmospheric turbulence introducing a disturbance in the secondary DM command, and the advantage with respect the phase screen is that it's possible changing in a simple way a lot of parameters, like seeing, wind speed and direction, atmospheric layer heights, the length of the largest eddies (L0) that describe the spatial statistics of a turbulent flow [A:N.Kolmogorov 1991]. In fact the dimension of the pupil on the phase screen corresponds to a seeing value "s" (i.e. 5mm diameter pupil means 0.4" of seeing), so in order to obtain a high value of seeing we have to increase the pupil dimension but it's evident that it's a constraint; so if we want to check the behavior of the system using a new configuration of atmosphere parameters we need a variable optical set-up that is able to change

the pupil dimension each time is required, and it's not easy to obtain because of the not much available free space on the AGW.

The Phase Screen (PS)

Despite these problems, at the beginning we though about using a phase screen, positioned on the incoming beam toward the secondary mirror. The behaviour of PS is very simple: it rotates around its axis, and because of the roughness of its mirror surface it introduces on the pupil image projected onto it, some 'disturbs' on the incoming wavefront, very similar to the ones introduced by the presence of the atmosphere.

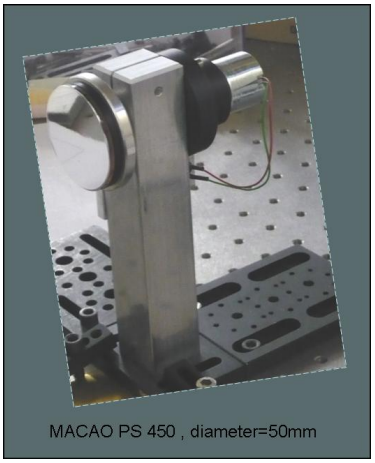

Figure 2.17: The phase screen

The Phase Screen inside the AGW optical system

The Arcetri tests of AGW AO system has been made using a reference source, located in the auxiliary unit. The beam coming from it is directed to the optical board by a cube beam splitter. The PS was positioned into the free part of the auxiliary unit (the opposite one respect to the fiber source). In the picture 2.18 is shown the position of the phase screen inside the system.

The cube beam splitter has three possible configurations:

- The 'nominal position' that sends the beam reflected directly to

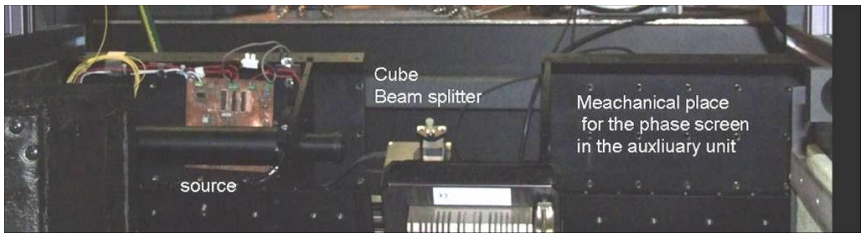

Figure 2.18: Into the auxiliary unit an optical system, that forms a pupil with the right dimension on the phase screen.

the optical board. The transmitted part toward the phase screen is obscured by a cover.

- A position rotated by 90° from the nominal one that allows the beam to go in transmission to the phase screen, and sends the beam, reflected by the phase screen, toward the board.

- In a third position the cube is rotated and translated , so that the beam reflected by the phase screen is sent to the secondary mirror and comes back in axis with the board. Using an appropriate position of the cube, we can separate the first reflection from the beam reflected by the phase screen because the first one is tilted away.

We can switch between the three configurations just by remotely rotating and translating the cube.

The separation between the beam coming from the nominal position and the beam coming from the secondary mirror reflection is required, in order to input in the optical board only the interested beam for the analysis, and so only the beam passes through the phase screen and arrived from the DM. Some simulation (by Zemax) has been made in order to analyze the behavior of the phase screen inside the AGW system. In the figure 2.19 the simulation optical design set up of the phase screen inside the system is shown.

By the simulation we obtained a separation of the beam coming from the first reflection, with respect to the beam coming from the secondary mirror, of 4.5mm measured on the exit side of the cube, and thanks to this setup is

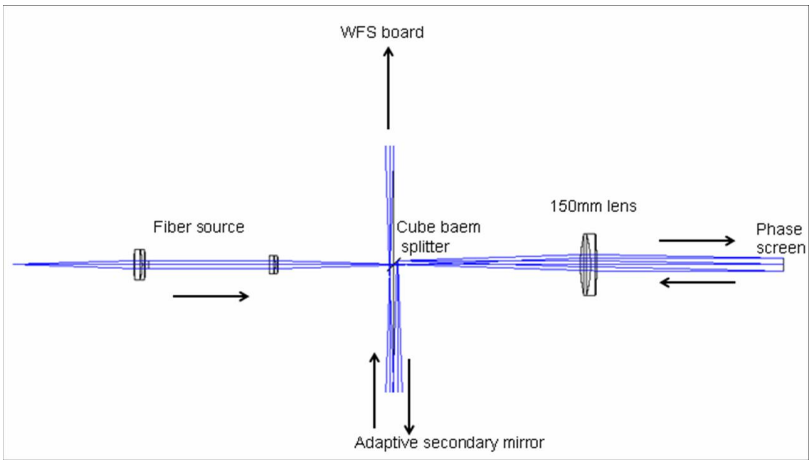

Figure 2.19: A Zemax optical design of phase screen in the AGW system set-up.

therefore possible to have only the relevant beam entering in the board. In order to obtain it the cube is been rotated and translated of 0.02° and 3mm respectively.
We can see that is a values are very near to the effective accuracy of the cube, so it represents another problem in order to use the phase screen as simulator of the atmosphere for this AO system.

The atmospheric disturbance introduced as a disturbance command vector

For the two main problems described in the previous paragraph, in the Solar Tower Optical Bench we do not have comprised a rotating phase screen emulating the time-evolving atmospheric turbulence, while . Instead, the atmospheric disturbance is introduced in the optical path by the AdSec unit itself with a disturbance command vector that is added at each loop iteration to the final position command (see [F.Quirós2009]), in order to have an equivalent seeing of 0.8 arcsec (r0=12.6cm @ 500nm).

2.4 The Arcetri Solar tower system set-up

In the Arcetri solar tower the whole AO system has been reproduced, in order to test it before its collocation at the telescope. LBT is a double reflector telescope, and the two branches form two independent AO system, and we have considered only one branch of it reproducing in the solar tower, obtaining

an environment similar to the telescope.
In the original configuration at the telescope, the beam from sky is focused by a primary mirror M1 in a focus point F1, that is the same of the first focus of the elliptical surface of the secondary DM, so the beam is directed toward the F2 of SDM or, thanks to the M3 toward the WFS board. In the solar tower we obtained the same 'effect' of the M1 using a double pass configuration: a reference source inside the flowerpot in the AGW generates a ≈F/14.5 beam and its focused is on the cube beam splitter, that sends a part of the beam on the secondary DM. These beams goes to the F1 of the SDM, and after toward a flat mirror, from it the beam follows the same optical path again (thanks to this reason it's called 'double pass configuration') until a dichroic window splits the beam toward the WFS board and toward the InfraRedTestCamera (IRTC, that is instead of Lucifer). The IRTC is based on a commercial IR camera, built by Observatory of Bologna, by a system of three lens it's possible to change the field of view (3,6 and 30 arcsec), two commercial filters are included in the design with band-passes 1050-1100 nm and 1500-1700nm (including the detector response cut-off at 1700nm), they are mounted on a positioning system ([S.Esposito & al. 2009]).

These tests are very important because we can check the AO system all together in the real work-condition as at the telescope: the secondary DM on the top of the solar tower, the AGW (so the pyramid wavefront sensor) on the bottom of the solar tower, and the IRTC analysis on the bottom of the solar tower too.

The tower tests, taking into account of some error contributions [F.Quirós & al. 2009], are able to check the performances of the whole AO system in the condition as similar as possible to the telescope. So the main tests are:

- system integration and alignment of of LBT672 and W unit.
- Calibration and closed loop test
- Installation and alignment of infrared test camera IRTC.
- Complete calibration of AO system. Optimization of system configuration to achieve the best SR

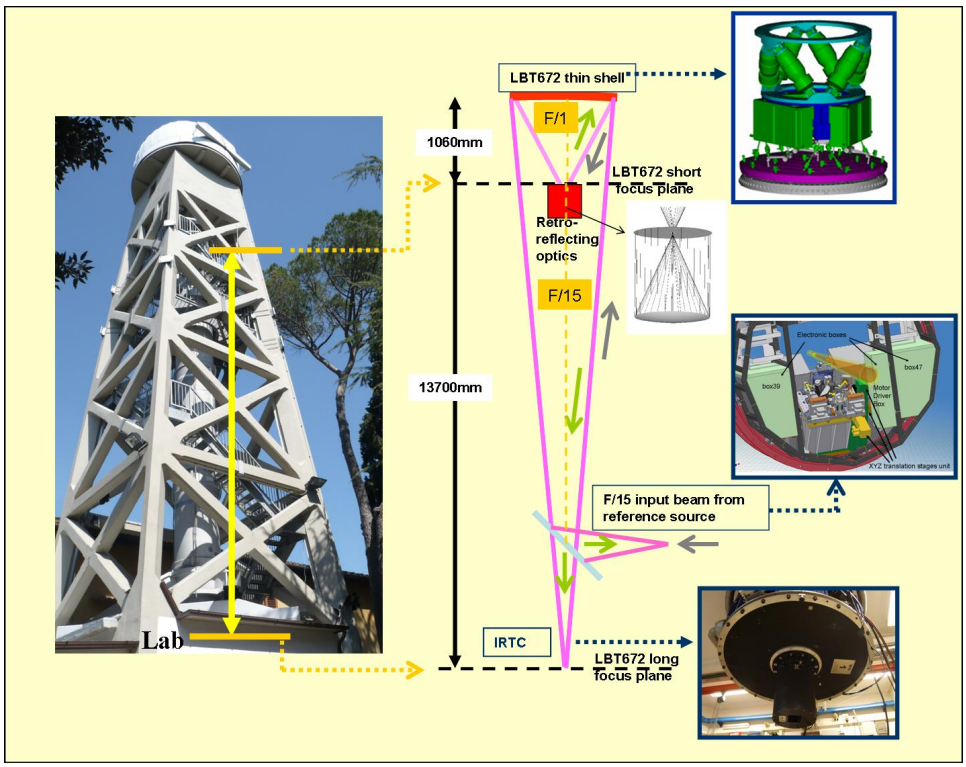

Figure 2.20: left:picture of the solar tower in Arcetri; right: a simplified scheme of the whole AO LBT system, with the incoming beam from the fiber source toward the SDM, and the outgoing beam from the DSM split toward the wave front optical system board and the IRTC.

In the meantime the AO system control software is been implemented.

Chapter 3

LBT calibration system

3.1 The AO system calibration

As we can see from the fundamental steps of solar tower tests (previous chapter), the first one, after the system assembling, is the calibration of the AO system. In fact, during observations, the AO system must be able to correct the atmospheric effects on the image seen by the telescope, working in closed loop to have a fast tracking of continuously changing atmospheric turbulence, in order to obtain a diffraction limited image starting from a seeing limited one. Using the pyramid sensor we can detect errors on the incoming wavefront, the secondary deformable mirror can compensate an arbitrary wavefront assuming an opposite shape (so that the result wavefront is flat): it needs a calibration procedure in order to connect WFS board signals to deformable mirror, it's like "setting a language between them".

Thanks to that, during the observation we can give real-time commands to the mirror to correct the incoming wavefront aberration (see figure 3.1).

The Interaction Matrix (IM)

In this phd thesis work we talk about calibration method and so about measuring interaction matrix, and so we want to introduce it also on mathematically point of view.
The theory of pyramid wavefront sensor with circular modulation ([S.esposito & al. 2001],[A.Burvall & al. 2006]) gives us the possibility to obtain an extimation of the aberration on the wavefront starting from the signal

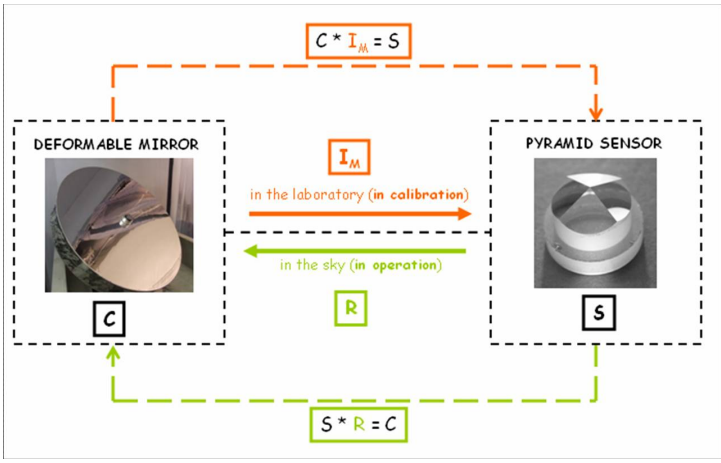

Figure 3.1:

recorded by the sensor:

$$\frac{\delta W}{\delta x} = \frac{R}{f} \sin\left(\frac{\pi}{2} S_x\right) \tag{3.1}$$

In the equation (3.1) f is the linear distance between the system exit pupil (located on the tip-tilt mirror) and the nominal focal plane, and R is the linear tip-tilt modulation radius again in the focal plane (see figure 3.2). The same equation (3.1) is obtained for signal y.
We don't know the aberration function and so it needs a reconstructor that is able to express the slopes measured by the sensor as a spatially continuum representation of the wavefront sensor itself. We have two different approach: finding a *Zonal Reconstructor* that gives an estimation of the wavefront in all point connected with the mirror actuators, and a *Modal Reconstructor* that gives the coefficients associated to the pupil function which the wavefront is decomposed (i.e. Zernike polynomials). The last one is better because less sensible to noise propagation of wavefront ([W.H. Southwell 1980]), for this reason we make use of it.

We need a spatial reconstructor of the wavefront, that have to be compensated by the deformable mirror thanks to the measured done by the wavefront sensor, and we can express it:

$$\widehat{a} = Z^{+} s \tag{3.2}$$

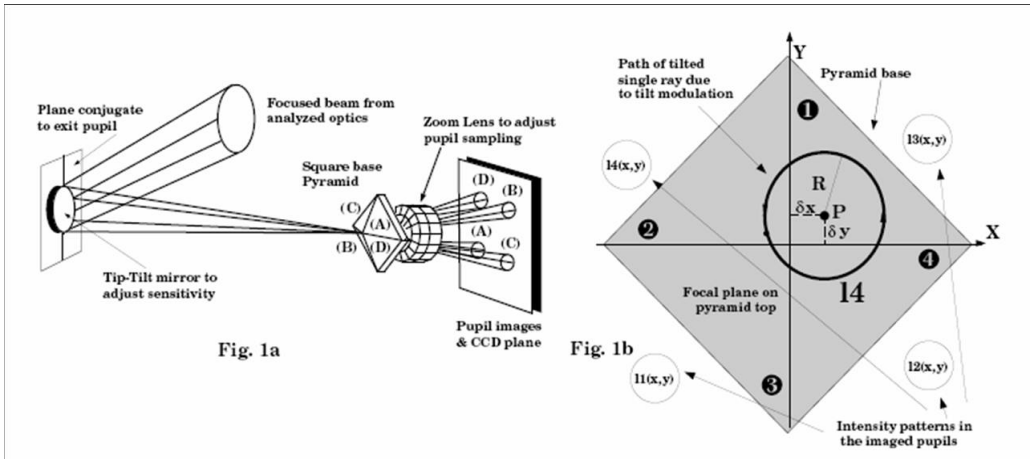

Figure 3.2: left: pyramid sensor principal elements. right:effect of tip-tilt modulation in the focal plane.

In the equation 3.2 $\widehat{a}$ is the coefficient modal vector by which we obtain the command vector to apply to the mirror, Z^+ is the reconstructor matrix and s is the signal vector measured by the waveferont sensor. We want obtain Z^+. We can start supposing that we are able to express our distorted wavefront by an orthonormal polynomials base, i.e Zernike polynomials ([R. J. Noll 1976]), so the wavefront base become:

$$\phi(x,y) = \sum_{i=1}^{k} a_i Z_i(x,y) \tag{3.3}$$

In the equation 3.3 a_i and Z_i are the i-polynomial coefficient and the i-polynomial associated respectively. From this equation we can give an estimation of wavefront gradient in x and y direction:

$$\frac{\partial\phi(x,y)}{\partial x} = \sum_{i=1}^{k} \widehat{a_i} \frac{\partial Z_i(x,y)}{\partial x} \tag{3.4}$$

and for the y direction:

$$\frac{\partial\phi(x,y)}{\partial y} = \sum_{i=1}^{k} \widehat{a_i} \frac{\partial Z_i(x,y)}{\partial y} \tag{3.5}$$

In both equations $\widehat{a}$ is the coefficient modal vector to find by which we obtain the command vector to apply to the mirror. We obtain a system composed of $2n_s$ equations, where n_s is the number of sensing zone of the system,

of K-1 unknowns (K is the order of polynomial), and we can re-write as matrix equation:

$$s = \sum_{i=1}^{k} Z_i \widehat{a_i} \tag{3.6}$$

In the equation 3.6 Z_i is the *Interaction Matrix* (IM) and is composed by the polynomial gradients and its dimension is $2n_s$xK. The column of this IM will be formate by all the signals generated by each mode that describe the wavefront it self.
At this point we can write the IM through the mirror control signals (by an opportunity matrix multiplication), making sure it maps the mirror space with the wavefront sensor space. The equation 3.6 can be resolved by the minimum square method, and the solution can be found reversing it:

$$\widehat{a_i} = \left(Z^t Z\right)^{-1} Z^t s = Z^+ s \tag{3.7}$$

We have found the Reconstruction matrix by the general inverse of the Interaction matrix. We can understand now that founding the IM is a fundamental step for adaptive optic systems.

3.2 The calibration step of AO system

3.2.1 The classical calibration technique

There is a simple way to measure the IM: it's to push each singular actuators one after other and measure the corresponding response vectors of the WFS, observing an artificial source located in the focal plane before the DM in the optical train; this is called the 'classical technique' of calibration, and is a zonal matrix. There are some problems in order to applied this technique to AO system with many actuators, both in time required for measuring the total IM, and in the introduction of some optical disturbances because of the large distance between the WFS and the DM, that could introduce local turbulence along the optical train. Several telescopes of 8m class using a large deformable secondary mirror, both in size and in the number of actuators, furthermore most of the AO system planned to be installed on an European ELT should be using a very large secondary DM, more than one meter and spatially

sampled by more than 1000 actuators. For all such telescope the AO system calibration using a reference fiber as AO system reference source can be very difficult or impossible. We can easily understand now the reason of founding new solutions to estimate the IM. This topic has been studied by some authors [M.Kasper & al. 2004], [F.P. Wildi & al.2004], [S. Oberti & al.2006], [S. Esposito & al. 2006], [F.Pieralli & al.2008], that for explained the reasons to investigate new calibration techniques for IM construction for the case of very large telescopes, like MMT [F.P. Wildi & al.2004],
VLT [S.Stroebele & al. 2006], LBT [S.Esposito & al.2006].

3.2.2 The new calibration techniques

There are two techniques that can be used instead of the classical one: the 'push pull' technique and the sinusoidal modulation technique, that aimed at performing measurement of AO system interaction matrix in noisy environment or, only in case of the sinusoidal modulation technique, also on sky.

The push pull technique

An easy method in order to avoid the atmospheric noise is to use an exposure time sufficiently short in order to consider the atmosphere as frozen in it. This method it's called 'push-pull' method, in fact each mode is measured for some milliseconds (at about 5ms, and the setting time of the secondary mirror il less than 1ms) with an amplitude 'a', and some ms with an amplitude '-a', the next step is to subtract the two measurements, in order to delete all local turbulence effects and low frequency drift (like variation of temperature,DM creep..).
The push-pull technique can be used to calibrate one mode at a time. The j^{th} column of the interaction matrix containing the WFS signal vector S associated with the th mode (m_j) was computed as:

$$IM_j = \frac{S(+Am_j) - S(-Am_j)}{2A} \tag{3.8}$$

In the equation 3.8 A is the amplitude factor. It is important to recall that higher signal amplitudes are expected from higher-order modes due to their stronger local gradients. Hence, the amplitude A should be reduced for

higher-order modes in order to prevent WFS signal saturation [F.Quirós2009]. The push-pull technique is very good applied to open loop measurements, because it is able to measure an IM matrix in very short time compared to the classical one. In fact by classical method, in order to avoid all local disturb we need some seconds for each mode, and so for the complete IM we need more then one hour. For LBT case we can choose among some frequencies loop (with a maximum of 1000Hz), for example if we use a frequency loop of 400Hz, we measure 10 frames (5 up and 5 down) for each mode, we repeat this measure 4 times (in order to obtain higher value of S/N), so we obtain a total time integration of some minutes for 672 modes. The limitation of the push-pull technique is represented by the measure of IM in presence of an atmospheric environment. In fact the turbulence effect began the fundamental component of each measurement.

Sinusoidal modulation technique

About the technique

We know that using the WFS we can detect the errors on the incoming wave front, thanks to the DM we can compensate an arbitrary wave front assuming an opposite shape in order to obtain a flat wave front, but only thanks to the IM we can link this two fundamental steps. So we can understand why it's very important that this process is affected as little as possible by several kinds of measurement errors. For this reason we want to apply the sinusoidal modulation technique to LBT system, in order to reduce all these sources of errors in the measurement of the calibration matrix.
This technique allows us to measure multiple modes at the same time. The concept is: to introduce a sinusoidal signal with a specific frequency, selecting a different frequency for each mode (applied at the same time), modulate each of these mode amplitude with its sinusoidal signal, sum all commands together, and apply the summed commands to the DM, and, as final step of measure, recording the sensor signal. After that there is the basic step of demodulation: the sensor signal is demodulated with the different frequencies injected (one for each mode chosen), in order to recover the single modes applied. The demodulation is equivalent to a narrow band pass filter which is able, at the

working frequency, to retrieve the modulated signal input.
It's important to remember that the modulation can be applied to several modes with different frequencies and each mode is demodulated independently, this multiplexing obviously helps to reduce the calibration time by a factor equal to the number of multiplexed modes. We can apply this technique in open or closed loop indifferently.

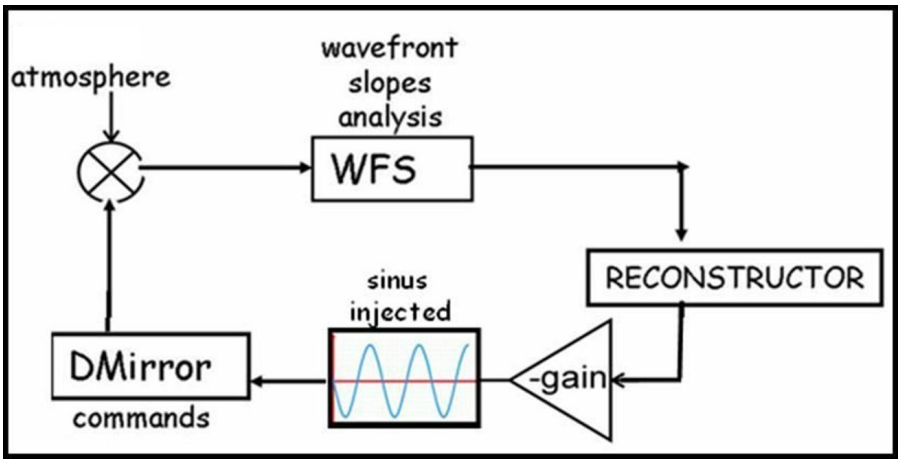

Figure 3.3: schema of close loop system, and where we can introduce the sinusoidal command disturb

There are two fundamental gains in applying this technique. Like the push pull technique, there is a reduction in time integration of about an order of magnitude (minutes required for IM LBT 672 modes instead hours by measuring it by classical method). The other gain is the SNR improvement thanks to demodulation that selects the bandwidth of the considered measure and allows us to move the measurement in a frequency range where the noise is less important, so that any noise at different frequencies from the one selected will be rejected by the modulation, and the detection bandwidth of the considered measure is moved from 0 Hz to the frequency of the sinusoidal command injected. This is very important because it is the reason we can apply the sinusoidal modulation technique also in closed loop IM measurement in presence of atmospheric turbulence, in fact selecting a very narrow bandwidth we can control the turbulence effects on the wavefront.

Mathematical description of the technique

The process of sinusoidal modulation technique can be written [S. Esposito & al. 2006] in formula defining a quantity Q(T) as follow:

$$Q(T) = \frac{1}{T}\int_0^T [S\sin 2\pi ft + B(t)]\, C\sin 2\pi ftdt \tag{3.9}$$

The quantity S and B are the sensor signal and the noise signal respectively, for a given subaperture; instead C is the injected command amplitude in mirror commands. Here we assume to inject a mirror mode into the system. With some easy calculation we can found:

$$Q = \frac{CS}{2} - \frac{CS}{4\pi fT}\sin 4\pi ft + \frac{1}{T}\int_0^T B(t)\sin 2\pi ftdt \tag{3.10}$$

There are three terms: the first one is the signal that we want to measure, the second one is the noise term, that easily goes to zero if we take T large enough, or however if we take an integer number of period. The third term is the real contribution to the noise measurement. We can see that this noise contribution is effective only in the noise spectrum at the considered frequency 'f'. We can rewrite the equation number 3.10 in the discrete formula in our discrete time domain:

$$Q_i = \sum_{k=1}^{N} \frac{[S_{i,k} + B_{i,k}]\, C_{i,k}}{\sum_{k=1}^{N} C_{i,k}^2} \tag{3.11}$$

Where $S_{i,k}$, $B_{i,k}$ are the sensor signal and the sensor noise respectively, and $C_{i,k}$ is the injected disturbance. All these values are evaluated at times t_i. The denominator is the normalization term for the IM. It is important to note that in the open loop case the measurements $C_{i,k}$ is the injected sinusoidal command at the DSM, while instead in closed loop $C_{i,k}$ is the closed loop mirror command, different from the previous case in amplitude and phase. In the discrete case we can easily see that the noise contribution will come from the noise power spectral density computed in the frequency bin f of width 1/T. Now it's important to underline that even if more than one frequency can be

used at the same time, there are two fundamental constraints: the saturation of wavefront sensor, and avoiding multiple frequencies.

3.3 Simulations of the calibration system applying sinusoidal technique

Simulations of the LBT AO system are required in order to set the best values of all the parameters that are necessary for the calibration sinusoidal technique. Both in open loop and in closed loop we have to explore the possibilities that allow us to obtain the best results. We start from the open loop case, and the best parameter obtained are the starting point for the closed loop case.

3.3.1 Simulation parameters

Some parameters are fixed and depend on the LBT system set-up: 8-meter class telescope diameter, secondary mirror of 672 actuators, and pyramid wave front sensor with 30x30 subapertures. The firsts simulations have been made to quantify the SNR and time integration achievable. We construct our IM in open loop applying different frequencies to different modes at the same time, and choosing frequencies not multiple of each other. A list of the parameters and their rationale follows [F.Pieralli & al.2008]:

- *Amplitude of injected sinusoidal signals.* The amplitude for each sinusoidal signal has to be adjusted in order to avoid saturating the sensor.

- *Frequencies of injected sinusoidal signals.* We have to choose frequencies vector with a sufficient quantity of periods inside the selected integration time, and, more importantly, without introducing aliasing effects.

- *Number of modes.* The number of modes that we can apply at the same time.

- *Integration time.*It must be long enough in order to achieve high SNR, and it also allows separating more clearly frequencies close to each other.

- *The magnitude of the reference source* In the laboratory we can assume a source as bright as needed (i.e magnitude=5). For the sky calibration, a sufficiently bright star should be selected (i.e magnitude=8).

- *The sampling system.* We use the maximum sampling possible, that is, the maximum number of subapertures allowed by the system.

In order to start the simulation we have to consider some constraints, strictly connected to the sinusoidal method applied: the aliasing effect between the frequencies (the cross talk affect), and the right amplitude to be applied to each mode.

3.3.2 The cross talk problem: choosing the right modulation frequency

Applying the modulation to severals modes with different frequencies at the same time we have to choose frequencies not multiple of each other, in order to avoid the aliasing effect. Since one cannot apply the whole 672 modes at the same time, some subsets must be chosen and the measure repeated with different subsets to complete the IM. The size of the subset thus strongly influences the total measurement time, and it's another free parameter so we repeated the measure for several different values of number of modes for single set (so for different values of integration time).
In order to quantify the cross talk, we evaluated the cross correlation between a sinusoidal signal at a frequency chosen, and all the other frequency with a sampling high enough in order to have more then 3 points of sampling in the maximum value (the pick of figure 3.4) of the Fourier transform of the sinusoidal signal. The convolution of the frequencies is evaluated inside the time integration selected. We can resume the mathematical fundamental equation of the convolution functions:

$$(f * g)(t) =^{def} \int_{-\infty}^{\infty} f(\tau) \cdot g(t-\tau) d\tau \tag{3.12}$$

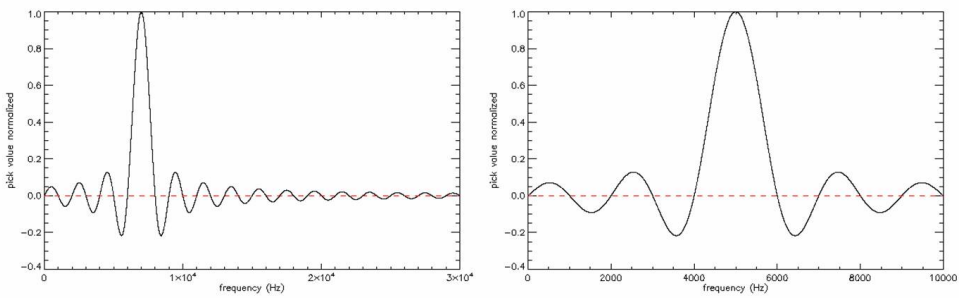

Figure 3.4: The convolution of the frequencies evaluated inside the time integration selected, on the left f(τ) and on the right g(t-τ), see equation 3.12.

For each time integration selected there is a function correlation result, and we can selected a threshold that corresponds to noise level, valuated in term of sigma multiply (3*σ) of the result. We overestimate the results if we approximate the correlation result function with a curve contained all the maximum values (as we can seen in the plot 3.5, green curve). Now we can select the minimum frequency difference like the intersection between the threshold and the maximum curve.
We can repeat this procedure for each integration time selected finding the minimum difference between the frequencies chosen, and they can be associated to the modes given at the same time.

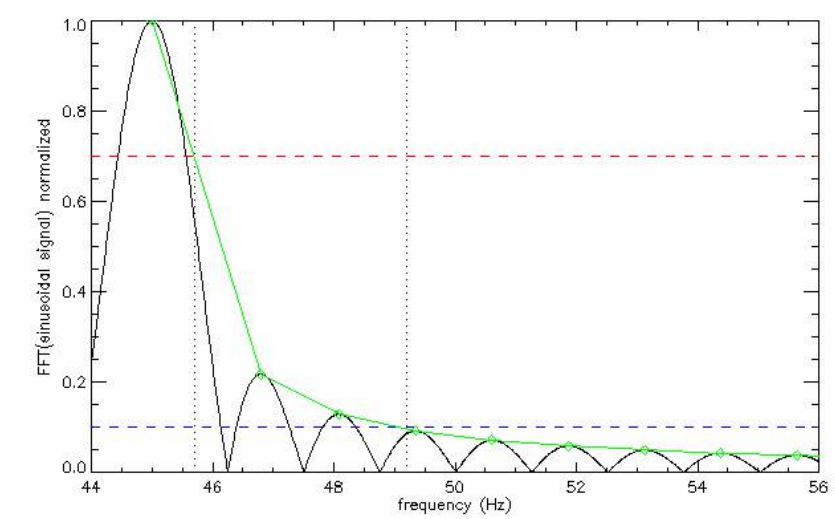

Figure 3.5: Exemple of correlation result between frequency of 45Hz and the other frequencies, valuated in the time integration of 4s. Gray line: fit of maximum values of curve result. Hatched lines: the two threshold selected, at 0.7 and 0.1. Black dotted line: the intersection between the threshold and the fit, that fixes the frequency range.

The integration time is another parameter, and its choosing it is strictly correlated with the minimum frequency range between each single frequencies of the modes measured at the same time, and it's the result of correlation between frequencies evaluated in that time. This parameter has to be chosen in order to reach the hight value of SNR in a time as short as possible. In the figure 3.6 we can see the behavior of the minimum frequencies range as function of integration time.

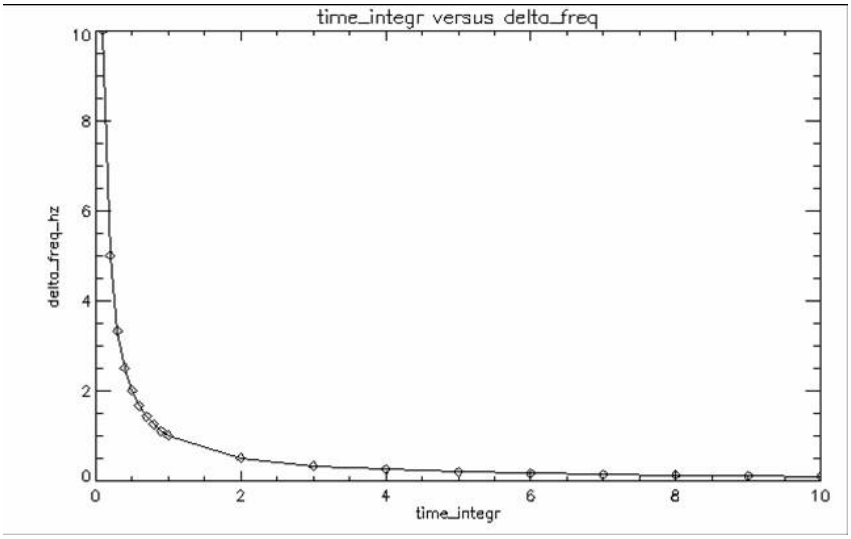

Figure 3.6: The plot is the integration time versus the minimum frequency value in order to avoid the cross talk, choosing the right frequency to give to each set of modes in the time integration evaluated. tme integration: from 0.1 seconds to 10 seconds, frequency values: from 0.1 Hz to 10 Hz

Another check of the results of cross talk correlation is the following: considering 50 frequencies that differs 1Hz one each other (so considering 50 modes), we construct a matrix value of the results valuated in cross correlation for each single frequency. The column of this matrix is the frequency selected (or the mode selected) correlated to the others.
Plotting this matrix the maximum values are represented by the diagonal line (figure 3.7), and its mean is simply the correlation of each frequency with its self; instead the minimum value found for each frequency is the best one, because it sees the minimum possible correlation, so the minimum cross talk.

From the figure 3.6 we know that in order to avoid cross talk for the case of 0.1 time integration, we need a frequency minimum range of about 10Hz,

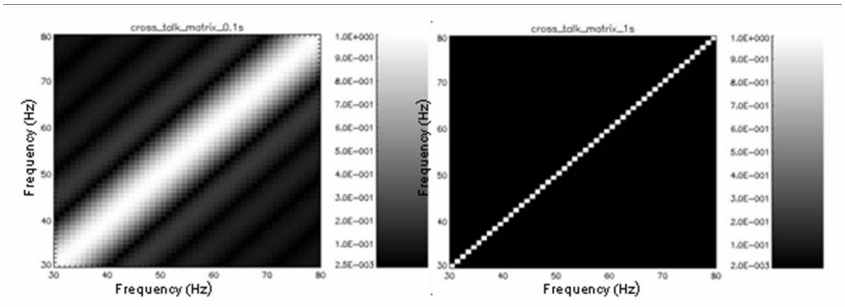

Figure 3.7: On the left: cross talk matrix valuated at time integration of 0.1s for 50 modes, starting from mode number 30 modulated at 30 Hz of frequency, to mode number 80 modulated at 80 Hz of frequency. Each mode has a frequency of 1Hz difference of the previous one. On the right: the same of left figure case but the matrix is valuated for time integration of 1s.

instead for 1sec is about 1Hz. This is in complete accord with the plot results in figure 3.7.

In order to choose the best frequency set, we have to take into account the behavior of the real systeme, analyzing as the linearity of the SDM as the behavior of the AGW optical board. In order to check it we give one single sinusoidal signal, at a frequency selected, as a disturbance, and we record the slopes vector results. If the behavior of the secondary DM is linear, and there are not any resonance frequency disturb by the AO board system, we'll find a peak at the frequency selected for our sinusoidal disturb (obviously we have excluded all the frequencies multiple of the chosen one that are involved in the cross talk effect).
We analyze the behavior of the DM introducing, one by one, sinusoidal disturbances associated to the mode number 0,150,300,408, and each one has been modulated with a frequency of 10,20,30,40,70,90 Hz respectively. We used more than one mode and more than one frequency, measured one by one, in order to obtain results that are independent from both, and it depends only from the AO system behavior.

From the analysis of each power spectral density of each frequency end mode case, we can see two peaks: the principal one of the modulation frequency, end another more lower peak at about 100Hz. In fact, after some tests, it has been found that the electronic guide of the camera lens on the board presents a frequency resonance at exactly 100Hz. Also after 10Hz there are a noise frequencies zone, that we avoid taking into account.

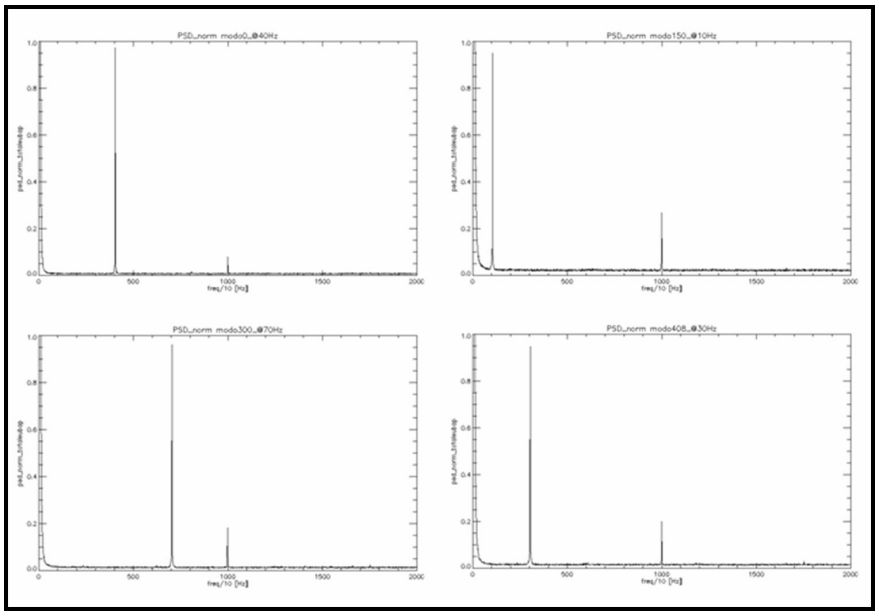

Figure 3.8: Starting from the left corner above and proceeding clockwise: the power spectral density of the signal recorded by the WFS, for the mode number 0 modulated at 40Hz, for the mode 150 at 70 Hz, for the mode 150 at 10Hz, for the mode 300 at 70Hz, end for the mode 408 at 30 Hz. All the plots presents the modulating frequency peak end also the peak at 100Hz.

3.3.3 The amplitude problem

The amplitude of injected sinusoidal signals is another fundamental parameter. Both the push pull method and the sinusoidal signal method has the same important constraint: the saturation of the pyramid wave front sensor.
We can start the best amplitude associated to each mode composed the IM measured by the push pull method. The next step evaluates the amplitude for the sinusoidal signal using a procedure that takes into account the constraint of saturation for the 'sum' of the modes given to the system at the same time.

The push pull amplitude

The first evaluation for the amplitude of each mode comes from the calculation of the maximum stroke that we can apply to the DSM for each mode. As first step the amplitude for each push pull mode has been scaled by a $1/\sqrt{n}$ factor, where n is the mode number ([F.Quirós2009]).
A more accurate measure of IM push pull, as function of amplitude value, has been optimized by analyzing the real measurements done by the tower cali-

bration system. In fact looking at the slope measurement of each single mode (used to construct the IM), it's possible to estimate how many signals are present between the two main limits: the upper one given by sensor saturation (this last limit is more restrictive then WFS limit of linear range or the DM limit force), and the lower one represented by noise. The last limit has been measured. We know that a certain amplitude corresponds to a certain amplitude of a given slope recorded for a selected mode; keeping in mind this we can measure the noise level of the system, keeping the DM still, and recording the slopes in the same system set-up of push-pull. We obtain a noise measurement of the system (without any kind of induced disturb), and sampling it in the same temporal sampling of the push pull method, we obtain our noise lower limit.
With these criteria we can evaluate, for each single mode, the best amplitude that maximizes the number of signals inside these two limits.
In the figure 3.9 there is an example of a recorded signals for one mode.

The sinusoidal amplitude

In order to find the best sinusoidal amplitude for each mode, we start from the best push pull results. We have the IM recorded and the noise level so we are able to calculate the S/N of the push pull integration matrix. Using this data and the noise level evaluated also for sinusoidal signal, we have written a procedure that can be summarized in these steps:

- Calculate the value of the SNR for the sinusoidal signals.
- We can re-scale the amplitude values of IM push pull modes, because we know the correspondence between given amplitude and slope measured for each single mode. We obtain the value of the sinusoidal amplitude for each mode (that have to give the slope value found at the previous point)
- Construct the IM sinusoidal with this amplitude, rescaling the push pull one measured.

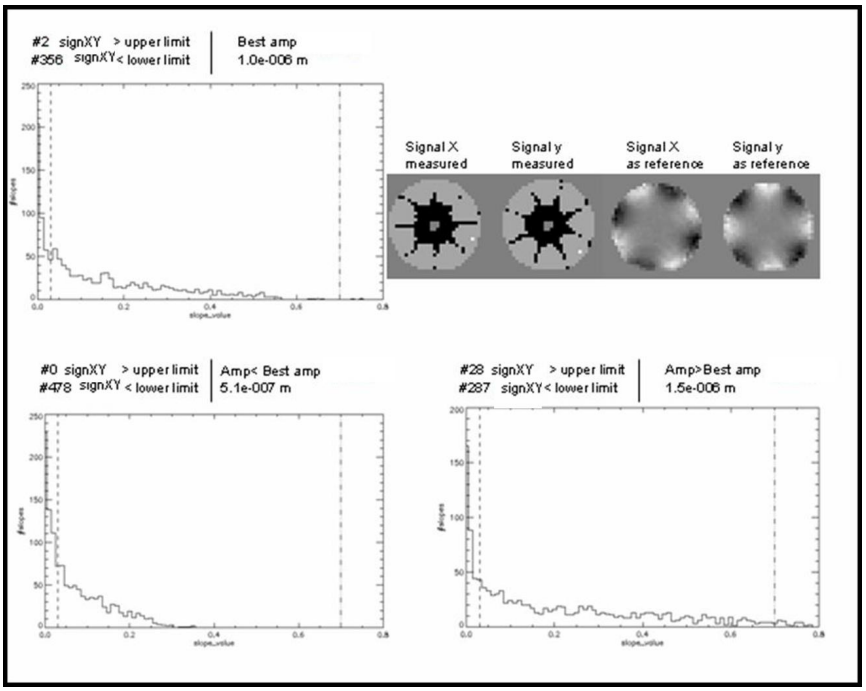

Figure 3.9: Example of the best value obtained for the mode number 10, analyzing the results of 10 IM, each one with different amplitude. Upper figure on the left: the distribution of x and y signal measured applying the amplitude of 1 micron. Lower on the left: the distribution of x and y signal measured applying at this mode an amplitude value less then 1 micron (0.51 micron). Lower on the right: the distribution of x and y signal measured applying at this mode an amplitude value more then 1 micron (1.5 micron). Taking into account that the total number of signals recorded are 1220, the best result is the amplitude of 1 micron, that has only 2 signals over the upper limit, and about 350 signals under the lower limit.

The procedure also takes into account of main constraints in order to apply more then one mode at the same time: the saturation of the WFS Evaluated for the sum of modes. We also have to maximize the number of signals over the lower noise limit. From these two constraints we deduced the modes that we can put together in a single set of measure, each one with the 'best' amplitude.

Chapter 4

Data analysis

4.1 The *simulation results* of the push-pull and sinusoidal calibration techniques

The simulations are made in order to evaluate all possible kinds of problems applying all the parameters that characterized the sinusoidal signal, like amplitude and frequency for each single mode, or also the time integration or the residual value of each mode after SDM correction.
So, at first, all these steps are checked in simulation as best as possible, in order to have an idea of the behavior of the sinusoidal calibration method before applying it in the real case. We have to underline that each simulation case requires a lot of time, much more than real (i.e. hours instead of minutes in order to measure a set 10 modes modulated by sinusoidal signal), and so we have to restrict our analysis to the main cases.

4.1.1 The open-loop case

The first kind of simulation has been performed in order to measure in open loop a single mode modulated with a set frequency it's a simple check in order to understand the behavior of all the simulation procedure. So we measured some single mode without any kind of disturb inside the system, and in the figure 4.1 we can see the WFS signal patterns (2D display). We have used both the fast push-pull technique and the sinusoidal technique, and compare.

We measured 20 single modes, at first one by one, and modulating each one by three different frequencies, 20Hz,30Hz, and 45Hz. We evaluated the rms dif-

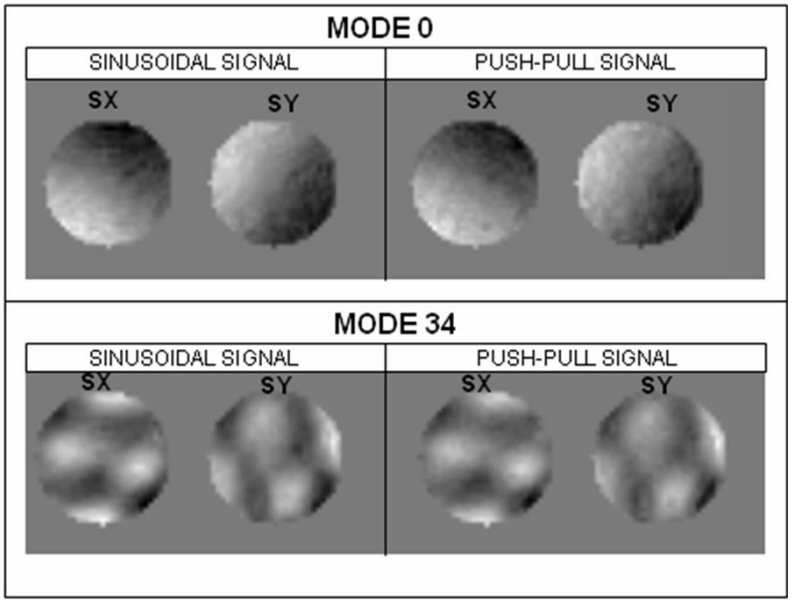

Figure 4.1: A 2D display of WFS signal X and Y, valuated for the mode number 0 and 34; each signal has been measured by the two method: push pull and sinusoidal, modulate at 45Hz

ference, for each single frequency case, subtracting the push-pull measure from sinusoidal one. Moreover, from the noise measurement threshold (explained in 'The sinusoidal amplitude' paragraph in chapter 3) we know that all the residual results below this value are comparable to noise, and so referring to figure 4.2, we deduced that all results for each frequency are comparable.

The second step was measuring the whole interaction matrix using both methods. A total of 671 (without piston) mirror modes were calibrated. The same simulation parameters are used in both cases, 400Hz of sampling frequency system, modulation radius equal to 3 (in lambda/D units), and a calibrating source of magnitude 5.
We obtain a measure of each mode, measuring it one by one in push-pull method, or measuring a set of 20 modes at the same time by sinusoidal method. At the end we are able to reconstruct the interaction matrix of 671 modes. The criteria in order to choose the modes that form each set are explained in the previous chapter (section 3.3). The starting frequency for the first mode of each set is 30Hz.
There is a criteria that allow us to evaluate the IM results. We know that we

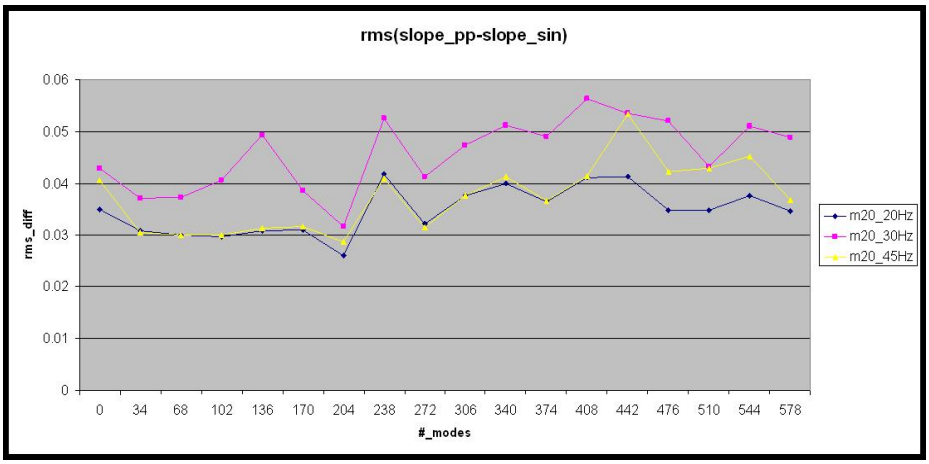

Figure 4.2: A plot of the difference between the rms signal measured by push pull method and the rms signal measured by sinusoidal method. Each color represents the value calculated for each single mode at a specific frequncy: blue at 20Hz, pink at 30Hz, yellow at 45Hz. For each frequency case we measured 20 modes, chosen ramdomly among the available 672.

want to invert the IM measured in order to obtain the reconstruction matrix: we can do this by using the singular value decomposition method (called: svd). By this method we are able to express the construction matrix as function of IM matrix measured, as in this formula:

$$R = IM^{+} = U * W * V^{T} \tag{4.1}$$

Where V has the same dimension of IM and its columns forms an orthonormal base in the modal space (like a set of orthonormal $''input''$ basis vector directions for R, these are the eigenvectors of R*R), W is a diagonal matrix composed by IM elements that represents the singular values (which can be thought of as scalar $''gain\ controls''$ by which each corresponding input is multiplied to give a corresponding output), and the columns of U forms an orthonormal base in the modal coefficients space (like a set of orthonormal $''output''$ basis vector directions for R, these are the eigenvectors of RR*). A common convention is to order the diagonal elements of W in descending order. In this case the diagonal matrix W is uniquely determined by R.
The meaning of the singular value calculation (the W elements from the equation 4.1) is that we are able to evaluate the WFS sensitivity to the corresponding mode each singular value is how the WFS sees the DM-mode considered. For example the lower bound is represented by the piston mode, that corre-

sponds to a singular value equal to zero. This means that the mode is completely not detected by the sensor. So, if the plots of the W values obtained by each method (push-pull and sinusoidal) are comparable, we can deduce (thank to the uniquely determination of W by R) that the reconstructors are similar and so the IM are similar too. Comparing the W of the two simulation results of IM obtained applying push-pull method and the IM obtained applying sinusoidal one, we can see that they are very similar (their maximum difference is under the noise level), as we can see in figure 4.3.

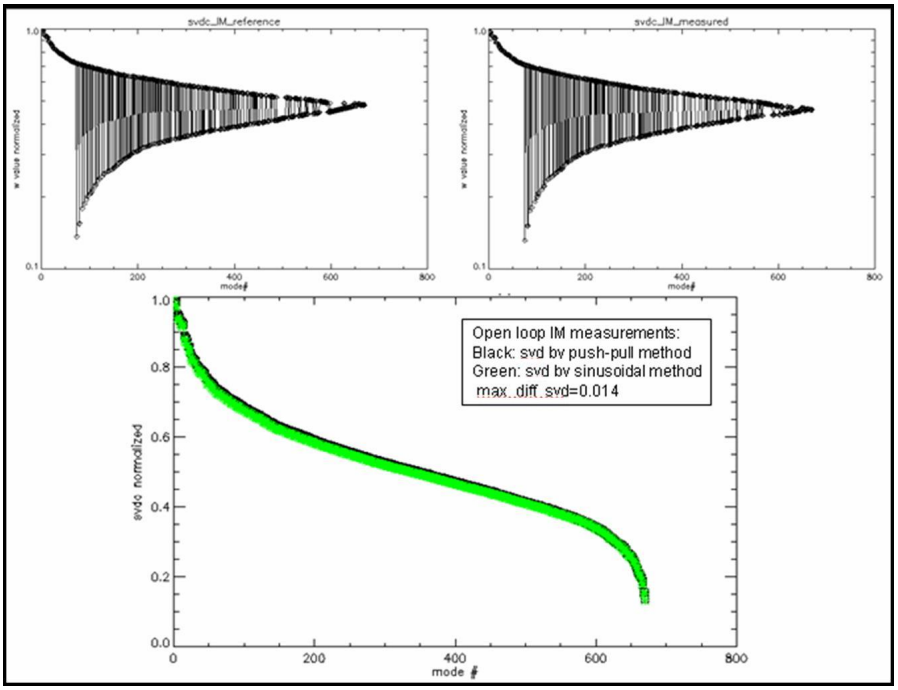

Figure 4.3: On the upper left corner the singular values of IM measured by simulations in open loop case by sinusoidal method; on the upper right corner the singular values of the IM measured by the push-pull method. A bottom central plot compares the two svd ordinated in descending order: black, singular values of open loop push-pull IM measure, green singular values of open loop sinusoidal IM measure.

The close loop with the measured IM

In order to check these results, we tried closing the loop using both the reconstruction matrix from the open loop measurements, one measured by the push-pull method and the other by the sinusoidal one, in both cases we have measured some modes, then compared the results.
We introduce the atmospheric turbulence and we want to see how the two

matrix are able to correct it. So we compare the measure of the signal modes measured by each closed loop.
In closed loop case we need to make attention to the possible mirror correction to the sinusoidal signal introduced by the modulation. It depends on the injecting frequency of the external sinusoidal disturb, and we are able to evaluate this attenuation of the amplitude injected by the mirror correction, thanks to the study of the RTF function of the system.

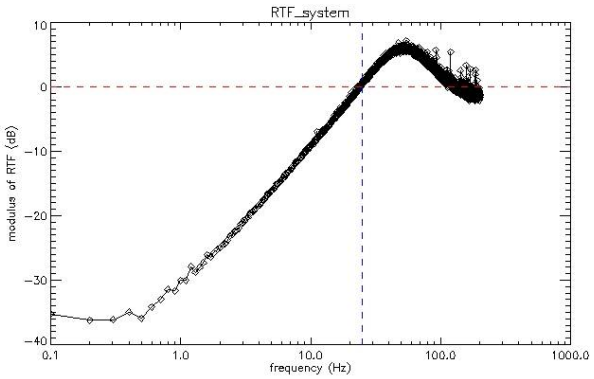

Figure 4.4: RTF evaluated at 400Hz sampling frequency, with modulation radius equal to 3 (in lambda/D units), injecting a frequency (by sinusoidal signal) equal to 25Hz, we obtain neither a reduction nor an amplification on the amplitude of the sinus injected at 25Hz.

We can *"resolve"* this problem in two ways: at first we can consider all the frequencies that are higher than a certain frequency, like 80Hz and more; or we can calculate the amplitude reduction or amplification at the selected frequency. Now we are sure that the sinusoidal disturbances applied as input disturbance is the same as the one used in order to demodulate the slope measured results.
In order to calculate the reduction or amplification factor we compare the injected sinusoidal signal with the closed loop residuals as seen from the wavefront sensor, figure 4.5. The latter can be computed subtracting the injected signal from the closed loop results. The ratio between the injected signal and the residuals can be obtained simply demodulating the second by the first, after correcting for the phase shift.

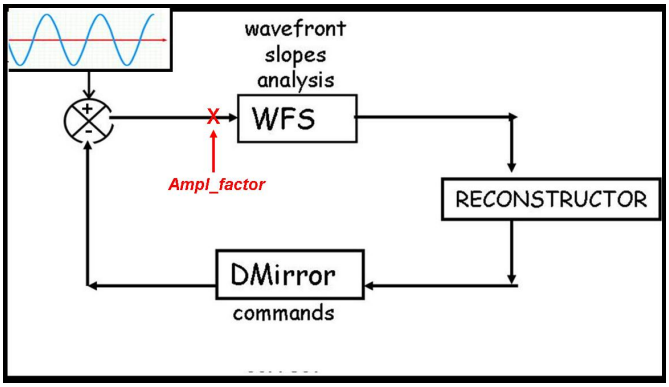

Figure 4.5: Schema of the closed loop system, the red 'X' point in the figure represents the point where we compare the injected sinusoidal signal with the closed loop residuals as seen from the wavefront sensor.

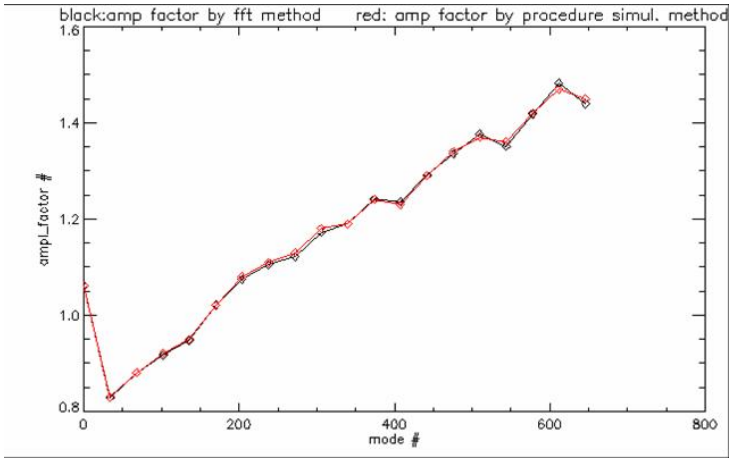

Figure 4.6: Plot of the amplitude factor obtained: black results by the fft method, comparing peak values at the injected sinusoidal signal and residuals at the chosen frequency; red results by comparing the injected sinusoidal signal with the closed loop residuals as seen from the wavefront sensor

A more robust method is two analyze both time series (injected sinusoidal signal and residuals) with an FFT, and comparing peak values at the injected frequency. This method is independent of phase shift. The amplitude ratio is:

$$A_{rate} = \sqrt{P_{res} - P_{sin}} \tag{4.2}$$

Now we can demodulate our closed loop results by the right sinusoidal signal with the right amplitude. In the next figure 4.7 we have measured a set of 20 modes in presence of atmospheric turbulence (the atmospheric simulation has been made in order to have an equivalent seeing of 0.8 arcsec, r_0=12.6cm @ 500nm, generated by a phase screen with the desired turbulence statistics),

closing the loop by the REC matrix obtained from the open loop measures, one applying push-pull technique and the other one applying modulation sinusoidal technique, compared them in terms of root mean square values.

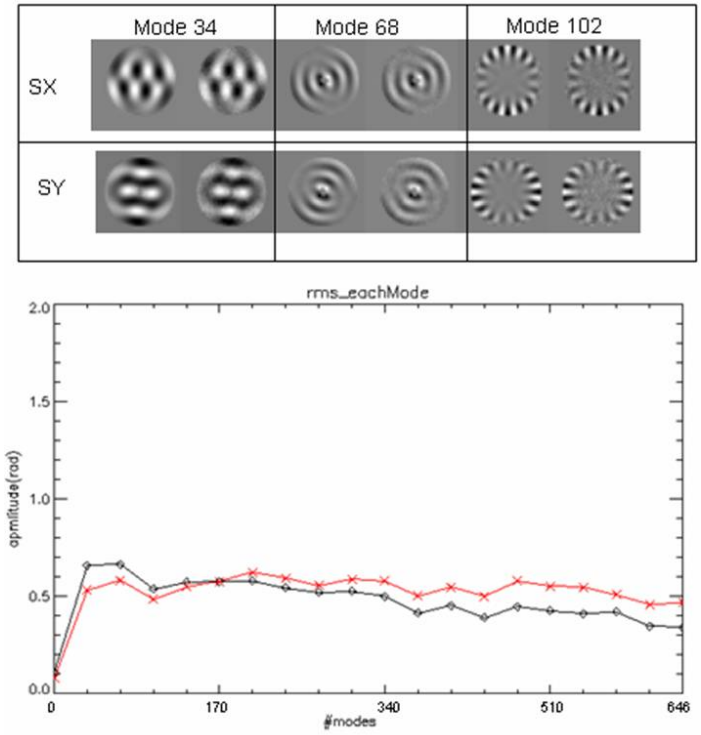

Figure 4.7: On the top: some modes (2D display) measured in closed loop, using reconstruction matrix measured in open loop with sinusoidal modulation method. At bottom plot of root mean square for each mode evaluated on all subapertures of the system, black: values calculated by results of closed loop with REC measured in open loop with push pull method, red: values calculated by results of closed loop with REC measured in open loop with sinusoidal modulation method.

4.1.2 Measure of IM in atmospheric turbulence environment (a closed loop case)

First, a premise: in this paragraph when we say that we want to acquire the interaction matrix measuring some modes, it's understood that these measures are done by applyng modulation sinusoidal technique. So each mode is modulated by a right frequency selected with a specific amplitude.

The measurements of IM in presence of atmospheric turbulence is the most

important case, because it allows us to measure the interaction matrix in presence of an atmospheric disturb, so directly on sky. The goal is to measure the IM *″onsky″* starting from any kind of simulation of synthetic interaction matrix [S. Oberti & al.2006], or also without the help of any IM obtained by laboratory open loop calibration of some lower modes (i.e. the first 10 modes on Karnuhel-Level polynomials base).
Before trying to apply this interaction matrix measurements directly by the solar tower AO system, we want to simulate it, in order to tackle all the possible problems that we could find, particularly selecting the right parameter, like tip-til modulation one.
Remembering that introducing a circular periodic modulation of the wavefront using the tip-tilt (TT) mirror the sensor sensitivity is changed. The sensor sensitivity is referred to the ratio between the sensor signal rms and the incoming wavefront rms. For a circular modulation TT, in case of the local wavefront tilt due to aberration is lower than the modulation radius, we can write [S.Esposito & al. 2000], by geometrical optical calculation [A.Burvall & al. 2006]:

$$\frac{\partial W}{\partial y} = \frac{R}{f} \cdot \sin\left(\frac{\pi}{2} \cdot S_y\right) \tag{4.3}$$

For small wavefront aberrations, and generally this is the case of closed loop operation, we can write:

$$\frac{\partial W}{\partial y} \approx \frac{R}{f} \cdot \frac{\pi}{2} \cdot S_y \tag{4.4}$$

In the equation 4.4, 'f' is the linear distance between the system exit pupil (located on the tip-tilt mirror) and the nominal focal plane, 'R' is the TT modulation amplitude (the radius) in the focal plane, and S_y is the wavefront sensor signal. The response functions S_y (and S_x) is proportional to the phase derivatives; the proportionality constant depends on the modulation amplitude R: increased modulation amplitude gives a decreased sensitivity. The pyramid sensor sensitivity can be adjusted depending on the starting aberration, and in closed loop the sensitivity can be increased as the wavefront sensor work goes ahead.

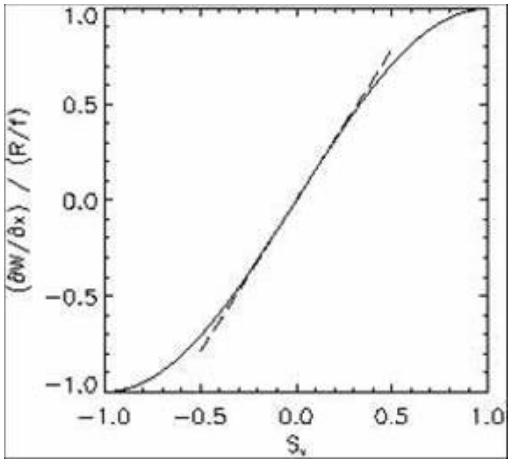

Figure 4.8: Plot: sensor signal (x axis) versus gradient of the wavefront aberration W(x,y) (y axis). The same is for the signal y. The value ±1 is the saturation threshold, the value ±0.5 is the linearity threshold for the pyramid WFS.

The first consideration is that, because of the presence of atmospheric turbulence, we need to consider most high modulation of the pyramid wavefront, in fact an increase of modulation radius implies a decrease of the sensitivity (see 4.4), and so we are less sensible to detect the larger aberration signals caused by atmospheric disturbs. By this we search about the modulation value that is able to detect our signal inside the saturation range of the pyramid wavefront: we try to detect only the atmospheric disturb by the pyramid WFS, putting any kind of other external signals (like the modulated sinusoidal one) inside the AO solar tower system, and we analyze the WFS signals detection.

We know now by figure 4.9 that using modulation more than $15(\lambda/D)$ we are able to measure our signals also in presence of atmospheric disturbs, keeping the signals in a range of no-saturation of the WFS in. Really we detect very low signals for this tip-tilt modulation radius, with a very low signal to noise ratio ($S_y \propto 1/R$), where R is the modulation radius. In order to improve this we have proceeded by iteration steps, and in each one we search about the right modulation: high enough to detect the signals also in atmospheric environment but, at the same time, it has to give a signal under the saturation threshold of wfs (typically under 0.5 in rad unit).

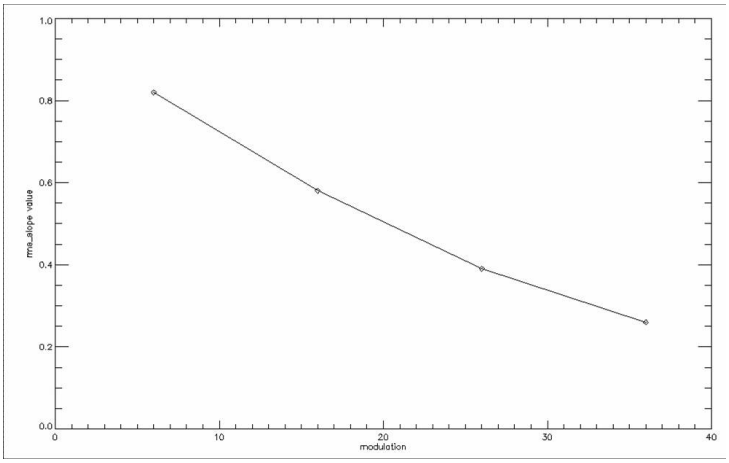

Figure 4.9: On x axis: the modulation value of,6,16,26,36 respectively; on y axis: the rms slope value evaluated for each modulation. we can see that as the modulation increase the rms slopes value decrease as expected by equation 4.4

The goal of this measure to obtain the interaction matrix directly on sky, so directly at telescope, without any kind of opening calibration. By this measure we are able to obtain an acquisition of the interaction matrix also for the telescope cases (most AO systems currently planned to be installed on a European ELT should be using a large adaptive mirror, more than 1000 actuators) where there is no possibility to obtain a calibration using a reference fiber illuminating both deformable mirror and wavefront sensor, because of the fiber-based IM measurements require challenging optical set-up that, in some cases, are unpractical to build.

We don't have any kind of interaction matrix in order to start our measures on sky, so the first step is to obtain some signals, i.e. firsts 20 modes, measured in open loop choosing the right modulation; thanks to this measure we obtain the *first interaction matrix*, and we are able to start our measure, i.e the firsts 10 modes, closing the loop by using this *embryonic IM*. This process is iterative: we start from the measure of these 10 firsts modes, but because of the atmospheric environment and consequently the high modulation that we have to apply, they have been characterizing by a very low SNR; we measure each step an higher number of modes, closing the loop by using the IM obtained by the previous measure (in closed loop), obtaining by these loop results a new IM composed by an higher number of modes. Thanks to this new IM we are able to correct better the atmospheric disturbs, the residual are lower and so

we can let loop modulation down, obtaining signals with an higher SNR.
The simulation are made in order to verify all this procedure measure by step. We have started by an open loop measure of the firsts 10 modes, and going on by steps that we describe as follow.
The atmospheric simulation has been made in order to have an equivalent seeing of 0.8 arcsec (r_0=12.6cm @ 500nm), A phase screen with the desired turbulence statistics (r_0, L_0) is generated.
The aim of the simulations is to understand the effectiveness of the method, and also the possible problems that we can find applying in really, so it's not fundamental to obtain the best results as possible. These simulations are a check in order to test the measuring method of the interaction matrix in a sky environment, and we want to test if we are able to obtain the results just as we expected.

STEP 0 OPEN LOOP

We need to measure the first set of modes (firsts 10 modes) in order to have a *″preliminary″* interaction matrix, and by it starting to measure our IM in closed loop.

We need a preliminary measure in order to select the best amplitude for the modes to be measured. We start from the best amplitudes founded for the push-pull case in the simulation results, and applying some different factors to them, we have made some different measures of the firsts 10 modes.

So we obtain the first measure of 10 modes in atmospheric environment by applying sinusoidal modulation signals with an amplitude equal to 0.6 push-pull amplitude. We called it: $IM_0^{OpenLoop}$.

STEP 0 CLOSED LOOP

Thanks to the open loop measurements of firsts modes, we have obtained the first IM, and obtaining by it the reconstructor, we can close the loop and measure the firsts 10 modes again, in the presence of atmospheric turbulence.

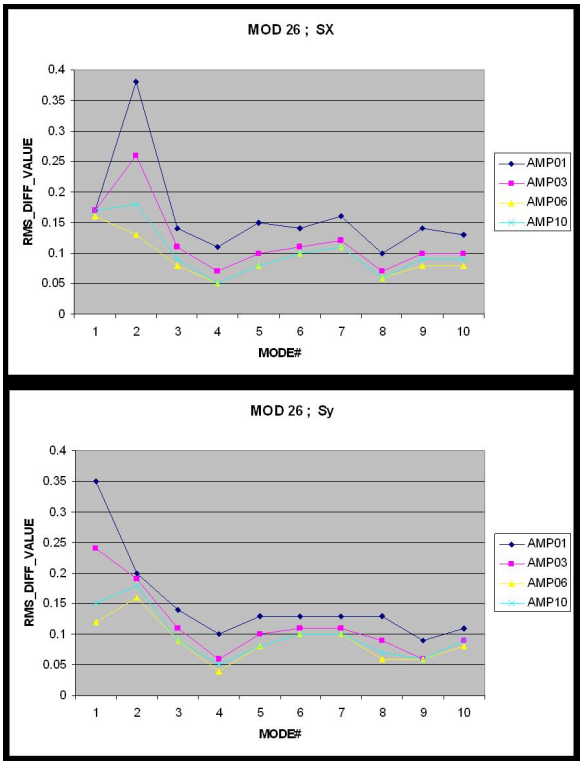

Figure 4.10: Open loop measurements of the firsts 10 modes. Each set is a different amplitude, and we have evaluated the root mean square (rms) difference between the signals obtained by applying the push-pull method in open loop, without any kind of atmospheric disturb, and the signals obtained by applying sinusoidal modulation method in open loop measurements but with atmospheric disturb. Blue: the sinusoidal signal applied to each mode has amplitude$_{sin}$=0.1*(amplitude$_{pushpull}$). Pink:the sinusoidal signal applied to each mode has amplitude$_{sin}$=0.3*(amplitude$_{pushpull}$). Yellow:the sinusoidal signal applied to each mode has amplitude$_{sin}$=0.6*(amplitude$_{pushpull}$). Light blue:the sinusoidal signal applied to each mode has amplitude$_{sin}$=1.0*(amplitude$_{pushpull}$). We have plotted the rms difference for both signals, Sx and Sy. For both cases the best results is the yellow line, in fact it has the lower rms difference values.

A modulation of $26(\lambda/D)$ has been used. The slopes result of single set of modes modulated by sinusoidal signal gives a mean value of 0.65 (it is the slope values as seen by the wfs, before the demodulation procedure, and also in the next step this number will be referring to it). From this measure we have obtained the first IM measured by closed loop of 10 modes. We called it: IM_0.

STEP 1 CLOSED LOOP

Thanks to the IM_0, by its the reconstructor, we can close the loop and

measure the firsts 20 modes, in the presence of atmospheric turbulence. A modulation of $26(\lambda/D)$ has been used. The slopes result of the two sets (of 10 modes each one) modulated by sinusoidal signal, gives a mean value of 0.54 for both. From this measure we have obtained an IM of 20 modes. We called it: IM_1.

STEP 2 CLOSED LOOP

Thanks to the IM_1, calculating the reconstructor, we can close the loop and measure the firsts 40 modes, in the presence of atmospheric turbulence. A modulation of $26(\lambda/D)$ has been used. The slopes result of the four sets (of 10 modes each one) modulated by sinusoidal signal, gives a mean value (valuated among the mean slopes results of each set) of 0.42. From this measure we have obtained an IM of 40 modes. We called it: IM_2.

STEP 3 CLOSED LOOP

Thanks to the IM_2, by its reconstructor, we can close the loop and measure the firsts 80 modes, in the presence of atmospheric turbulence. A modulation of $16(\lambda/D)$ has been used. The slopes result of the eight sets (of 10 modes each one) modulated by sinusoidal signal, gives a mean value (valuated among the mean slopes results of each set) of 0.30. From this measure we have obtained an IM of 80 modes. We called it: IM_3.

STEP 4 CLOSED LOOP

Thanks to the IM_3, obtaining the reconstructor, we can close the loop and measure the firsts 160 modes, in the presence of atmospheric turbulence. A modulation of $6(\lambda/D)$ has been used. The slopes result of the sixteen sets (of 10 modes each one) modulated by sinusoidal signal, gives a mean value (valuated among the mean slopes results of each set) of 0.24. From this measure we have obtained an IM of 160 modes. We called it: IM_4.

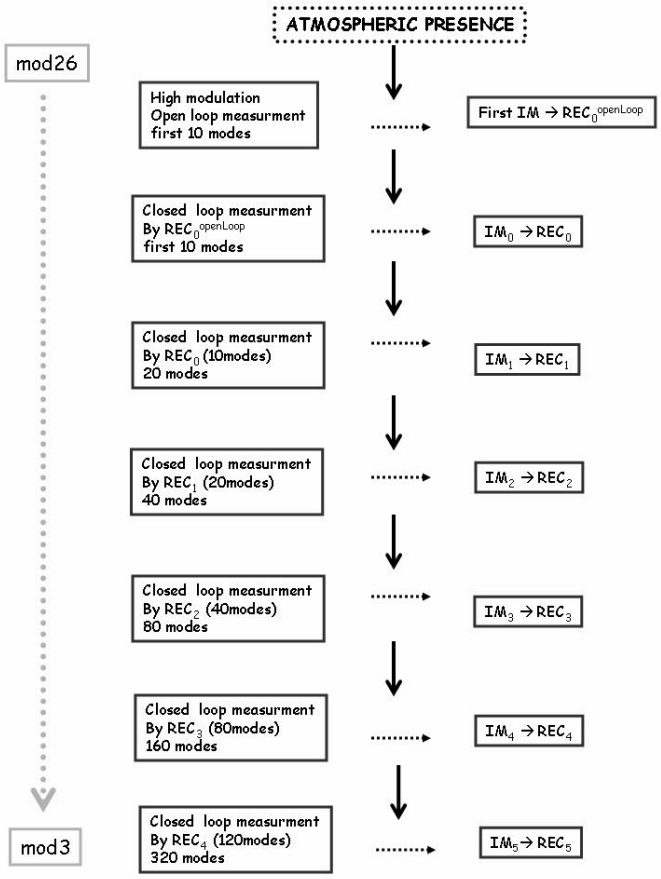

Figure 4.11: Schema of the simulation procedure in order to measure the IM in an atmospheric environment

STEP 5 CLOSED LOOP

Thanks to the IM_4, by its reconstructor, we can close the loop and measure the firsts 320 modes, in the presence of atmospheric turbulence. A modulation of $3(\lambda/D)$ has been used. The slopes result of the thirty two sets (of 10 modes each one) modulated by sinusoidal signal, gives a mean value (valuated among the mean slopes results of each set) of 0.22. From this measure we have obtained an IM of 320 modes. We called it: IM_5.

In the figure 4.11 there is a schema of the measure procedure.

We start by using a modulation equal to $26(\lambda/D)$ and we finish by using a modulation equal to $3(\lambda/D)$. The iteration process is able to obtain for each

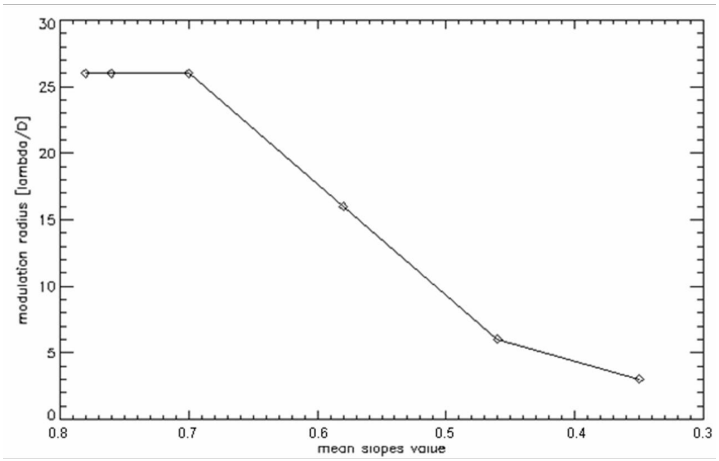

Figure 4.12: X axis: the mean slope value as seen by the WFS (before the demodulation procedure for each mode) of some modes measured in closed loop by using the IM derived, for each iteration, in the previous step (see description of single step above in this paragraph), always in presence of atmospheric turbulence. Y axis: the modulation radius of the tip- tilt applied for each step of measure.

step slopes having value below the saturation threshold of the pyramid sensor (lower than 0.5), and in the meantime, thanks to a lower radius of modulation applied, we obtain an higher SNR for each step of im measure.
We can deduce from this simulation that the behavior of the results, obtained by this method of measurements of IM in presence of atmospheric turbulence, is as expected.

By this first analysis we can deduce the good functioning of the method: we are able to measure the interaction matrix directly on sky, in an atmospheric disturb environment, starting from an open loop measurements of 10 sinusoidal modulated modes applying very hight modulation radius. At the beginning we obtain an IM with very low SNR (because of the high modulation) and with low mode number, but step by step we increase both, and at the end, we obtain an interaction matrix of more than 300 modes completely measured on sky, without any calibration procedure opening. In the next paragraph this method would be applied to the real case, in the solar tower AO system set up.

4.2 The *solar tower system measurements* of sinusoidal calibration technique

There were two steps of measurements in the solar tower system. So all the possible tests on this AO system are divided in two sections, and also the interaction matrix measures are split in two different time period, called $''PhaseA''$ and $''PhaseB''$. During Phase A of measures a preliminary comparison of the IM characteristics acquired with both techniques, push-pull and sinusoidal one. Phase B, trying to close the loop by these IM measured in phase A. In Phase B we have measured the IM with atmospheric simulated disturbance, which is the most interesting case.

4.2.1 The open-loop case

As in the simulations the first step was to measure some single modes, one by one, in order to start from the simplest possible case. We do not have any kind of disturb inside the system, and in figure 4.13 we can see the WFS signal patterns (2D display) as measured during these acquisitions on the solar tower system.
We have used both the fast push-pull technique and the sinusoidal technique, and compared thir results.

In order to measure the Interaction matrix in open loop, both by push pull method and by sinusoidal one. For this last case a set of modes (20) are applied at the same time, and modulated by different frequencies. The interaction matrices have been acquired for a total number of modes up to 600 for both cases. As explained in chapter 3, the following parameters for the IM acquisition have been explored, in order to optimize the performance of the sinusoidal technique:

- Ordering of the modes inside the set.
- The lower frequency of each set, in order to avoid disturbances induced by system vibration.

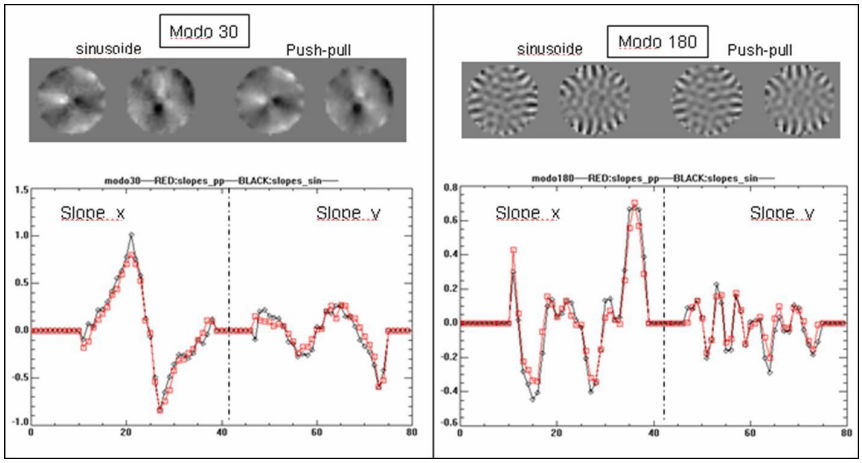

Figure 4.13: Measures of two modes, one by one, in open loop, on the left: 2D display results of mode number 30 measured by sinusoidal and push pull method, respectively black and red color on the plot containing the horizontal cut of the 2D display signal (valuated in X and Y direction in this plot). On the right: the same analysis on the mode number 180.

- The frequency of each mode inside a single set has been calculated in order to avoid the cross-talk between the modes.
- The mode amplitudes have been selected optimizing the signal on the WFS.

The results are plotted in figure 4.14. We can see that are comparable each other, the maximum difference is 0.05 that is very near to the noise level threshold (0.03-0.04).

Close the loop by the measured IM

The reconstructor matrices obtained from sinusoidal and push and pull techniques have been tested in closed loop in order to evaluate their performances (see figure 4.15). The closed loop has been performed with and without the disturbance simulating the atmospheric turbulence (seeing = $0.8''$, wind speed=6 m/s). By the simulation we are able to evaluate the reduction or amplification of the amplitude done by the closed loop mirror correction, and we know now that it depends on the injecting frequency of the external sinusoidal disturb. So we can demodulate our closed loop results by the right sinusoidal signal with the right amplitude, after correcting it for the phase shift.

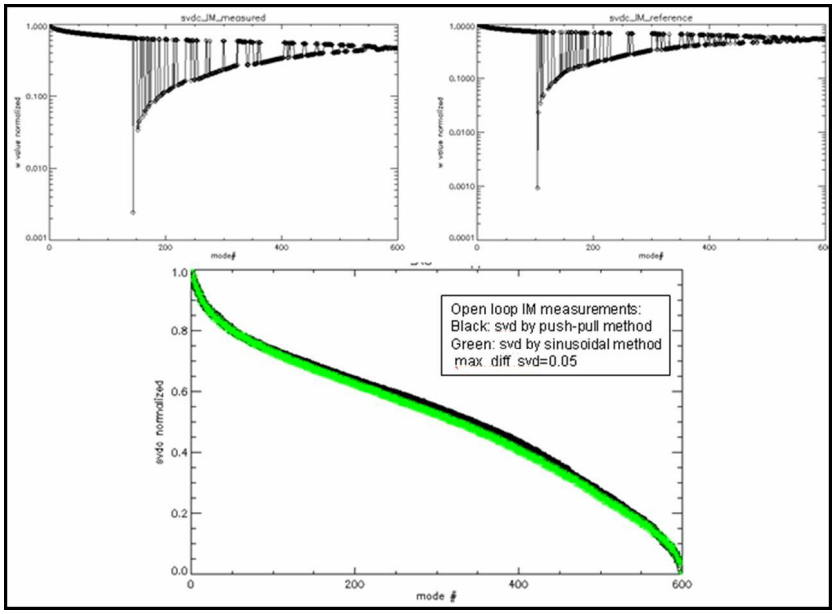

Figure 4.14: On the left corner the singular values of IM measured by solar tower system in open loop case by sinusoidal method; on the right corner the singular values of the IM measured by the push-pull method. At bottom central plot the compare between the two svd ordinated in descending order: black are singular values by open loop push-pull IM measure, green singular values by open loop sinusoidal IM measure.

4.2.2 The solar tower system measurements of IM in presence of atmospheric turbulence (closed loop case)

As first, the same premise as simulations: in this paragraph when we say that we want to acquire the interaction matrix measuring some modes, it's understood that these measures are doing by applying modulation sinusoidal technique. So each mode is modulated by a right frequency selected with a specific amplitude.

The goal was to measure the IM *on sky* (in an atmospheric environment) starting withouth any kind of simulation of syntethic matrix
([S. Oberti & al.2006]), and also without the help of any IM obtained by laboratory open loop calibration of some lower modes.
The atmospheric disturbance is introduced in the optical path by the AdSec unit itself with a disturbance command vector that is added at each loop iteration to the final position command [F.Quirós2009].
We have taken into account the same considerations of the simulation case. Remembering that, because of the presence of atmospheric turbulence, we need

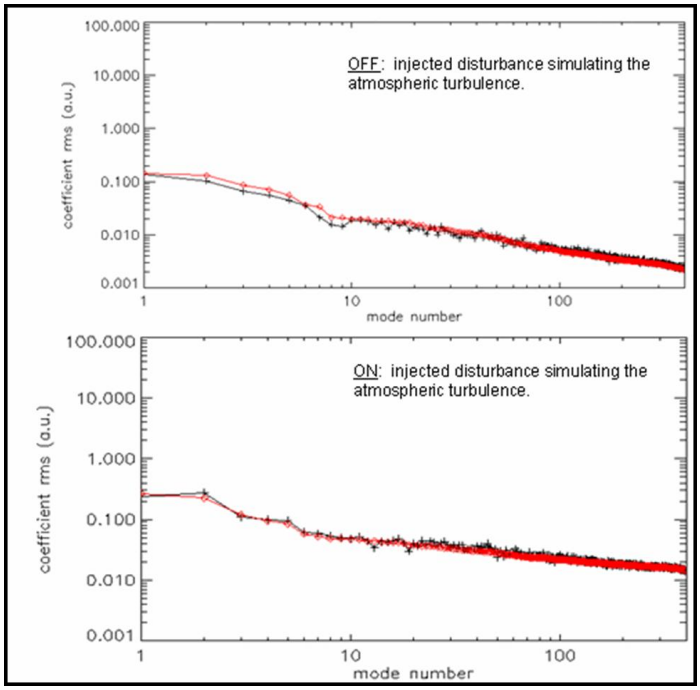

Figure 4.15: On the Top: signal modal decomposition for the closed loop using the sinusoidal reconstructor (black line) and the push-pull one (red line). This case is obtained correction 400 modes at 400Hz without any injected disturbance. On the bottom: signal modal decomposition for the closed loop using the sinusoidal reconstructor (black line) and the push-pull one (red line). This case is obtained correction 400 modes at 400Hz with an injected disturbance simulating the atmospheric turbulence.

to consider the highest modulation of the pyramid wavefront (see equation 4.3). We can see in figure 4.16 that as the modulation increase the rms slopes value decrease as expected by equation 4.4

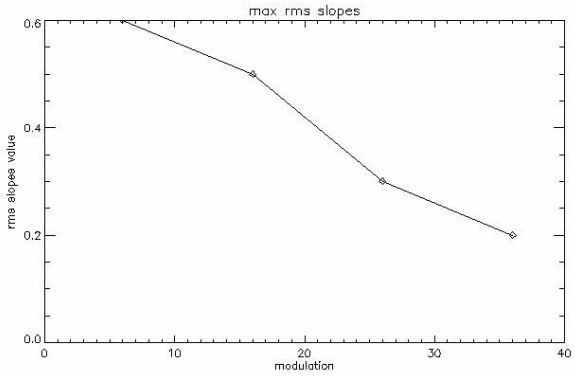

Figure 4.16: On x axis: the modulation value of,6,16,26,36 respectively; on y axis: the rms slope value evaluated for each modulation.

We proceed by the same method of simulation measurements: by steps. We have known by simulation that the first right modulation is about $26(\lambda/D)$, but in order to check the modulation value that is able to detect our signal inside the saturation range of the wavefront, we try to detect by the pyramid WFS only the atmospheric disturb (without any kind of other disturbs, like the modulated sinusoidal one).

In closed loop operation another parameter is the gain, it's represented by the value of the modal integrator, and for each modulation we want to find the maximum one that is able to keep stable the loop itself. The discrete transfer function for the integrator is:

$$C_s = g/s \tag{4.5}$$

In the equation 4.5 the integrator (expressed by the discrete transfer function C_s) is represented by the rate between the gain (g) and the signal measured by wavefront (s). If the signals are lower, because the modulation are higher (see equation 4.3), the gain has to be optimized consequently. For measuring the interaction matrix if the signals measured by wavefront are changed, it needs to change also the gain in order to obtain the right transfer function of the integrator.

We know now that by modulation equal to $26(\lambda/D)$ we are able to measure our signals also in presence of atmospheric disturb keeping them in a range of no-saturation of the WFS. Really we detect very low signals at the this tip-tilt modulation, with a very low signal to noise ratio. In order to improve this we have proceeded by iteration steps.

STEP 0 OPEN LOOP

We need to measure the first set of modes (i.e. the first 10 modes) in order to have a *preliminary* interaction matrix, to be used as a starting point for higher-order closed loop measures. We obtain the first measure of 10 modes

with atmospheric presence; we called it: $IM_0^{OpenLoop}$.
We have measured the first 10 modes with three different modulations: $26(\lambda/D)$, $16(\lambda/D)$, and $6(\lambda/D)$.
In order to evaluate the best result between the three IM (mod=$26(\lambda/D)$, mod=$16(\lambda/D)$, mod=$6(\lambda/D)$), we have evaluated the average slope value detected by sensor, after the demodulation step. We know that a mod=$6(\lambda/D)$ is probably too low, and so it will go out the saturation threshold of the pyramid sensor, but we want to check this.

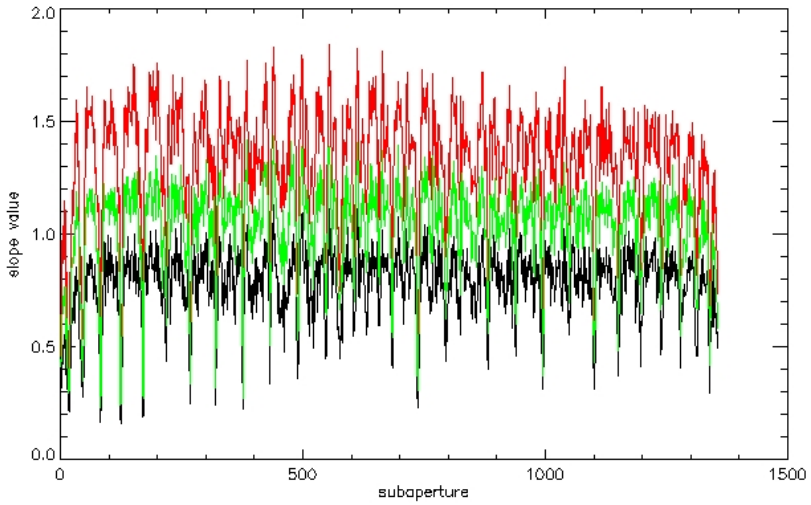

Figure 4.17: Evaluation of the average slope value detected by each subaperture on all integration time. Black: slopes signals detected at mod=$26(\lambda/D)$, with a mean slope value of 0.77. Green: the slopes signals detected at mod=$16(\lambda/D)$, with a mean slope value of 1.08. Red: the slopes signals detected at mod=$6(\lambda/D)$, with a mean slope value of 1.32.

From the plot 4.17 we deduce that both the modulation $16(\lambda/D)$, and the $6(\lambda/D)$, are too low as expected, in fact all the slope values are over the 1.0 threshold of saturation range for the WFS.

STEP 0 CLOSED LOOP

Thanks to $IM_0^{OpenLoop}$ measured we can close the loop using the pseudo-inverse of this interaction matrix, and we can measure again the first 10 modes. Because we are in closed loop, the WFS sees the residual of correction of the

mirror, and so the signals detected by WFS are now more distant from the saturation then the open loop case (the previous one), consequently the modulation can be lower (so the SNR is higher).
Two different modulations have been used: mod=26(λ/D), and mod=16(λ/D), so we obtain two different IM, one for each modulation. We know, from the plot 4.16, that mod=16(λ/D), probably is still too low in order to detect signals under the saturation threshold, but we want to test it on each mode measured.
As in step zero we have evaluated the average slope value detected by sensor, after the demodulation step.

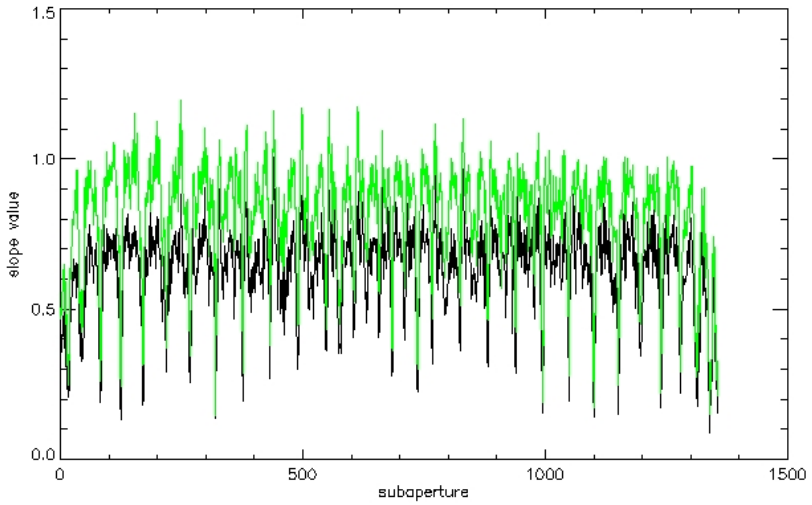

Figure 4.18: Evaluation of the average slope value detected by each subaperture on all integration time. Red: the slopes signals detected at mod=16(λ/D), with a mean slope value of 0.81. Black: slopes signals detected at mod=26(λ/D), with a mean slope value of 0.62.

From figure 4.18 the best result is represented by mod 26(λ/D), and in order to proceed with the next step, we construct the pseudo-inverse of this interaction matrix, called IM_1.

STEP 1 CLOSED LOOP

Thanks to the REC of IM_1 we can close the loop iterating our measures:

we want to detect now two sets of modes, each one composed by 10 modes (modulated by sinusoidal signal) at the same time. Three different modulations have been used: mod=26(λ/D), mod=16(λ/D), and mod=6(λ/D), so we obtain three different IM.

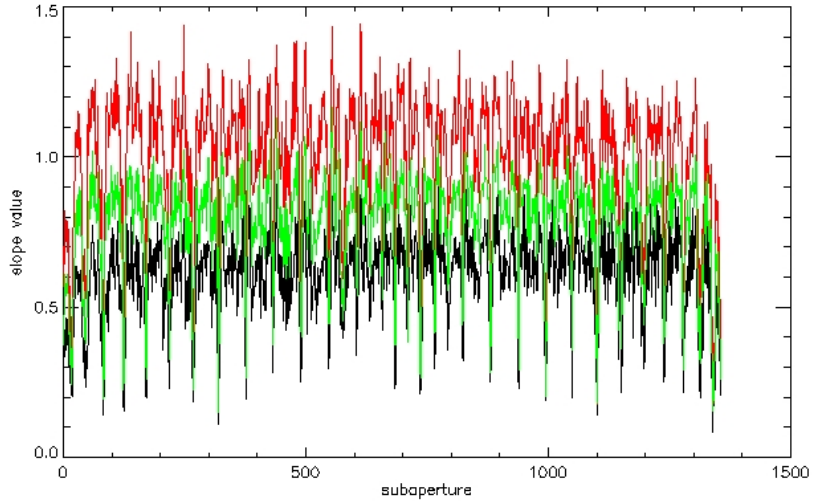

Figure 4.19: Evaluation of the average slope value detected by each subaperture on all integration time. Black: slopes signals detected at mod=26(λ/D), with a mean slope value of 0.65. Green: the slopes signals detected at mod=16(λ/D), with a mean slope value of 0.84. Red: the slopes signals detected at mod=6(λ/D), with a mean slope value of 1.10.

From figure 4.19 we deduce that the IM measures done by both modulations, 26(λ/D) and 16(λ/D), are inside the saturation range of pyramid WFS. The first one is still best result, and in order to proceed with the next step, we construct the the pseudo-inverse of this interaction matrix, called IM_2.

STEP 2 CLOSED LOOP

Thanks to the REC of IM_2 we can close the loop iterating our measures: we want to detect now more sets of modes (for a total of 110 modes), each one composed by 10 modes (modulated by sinusoidal signal) at the same time. Another time three different modulations have been used: mod=26(λ/D), mod=16(λ/D), and mod=6(λ/D), obtaining three different IM.

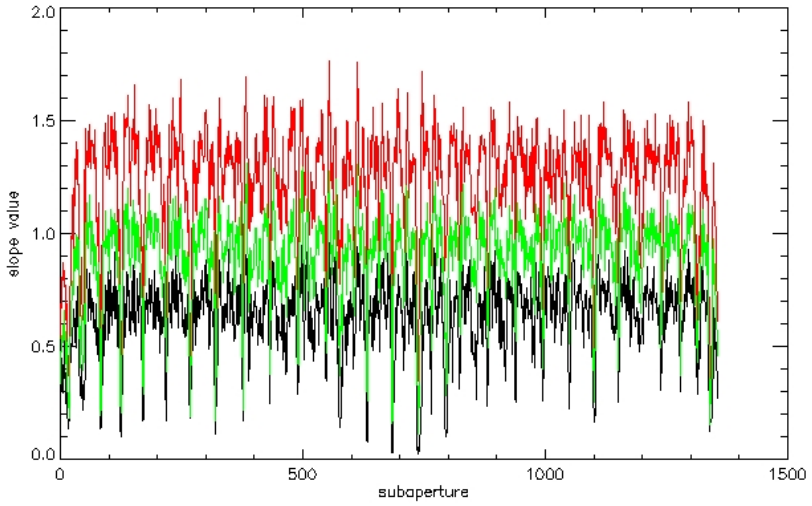

Figure 4.20: Evaluation of the average slope value detected by each subaperture on all integration time. Black: slopes signals detected at mod=26(λ/D), with a mean slope value of 0.62. Green: the slopes signals detected at mod=16(λ/D), with a mean slope value of 0.88. Red: the slopes signals detected at mod=6(λ/D), with a mean slope value of 1.22.

From figure 4.20 we deduce that the IM measures done by both modulations, 26(λ/D) and 16(λ/D), are inside the saturation range of the pyramid WFS. The two results are similar to the previous one (step 1) because now we have measured 110 modes with a REC matrix obtained by the correction of only 20 modes, while in the previous step 1, we have measured 20 modes with a REC matrix obtained by the correction of only 10 modes. In order to proceed with the next step, we construct the pseudo-inverse of the interaction matrix measured with modulation 16(λ/D), called IM_3.

STEP 3 CLOSED LOOP

Thanks to the REC of IM_3 we can close the loop iterating our measures again: we want to detect now 400 modes by sets composed each one by 10 modes (modulated by sinusoidal signal) at the same time. This time the different modulations used are: mod=16(λ/D), mod=10(λ/D), mod=6(λ/D), and mod=3(λ/D), obtaining four different IM.

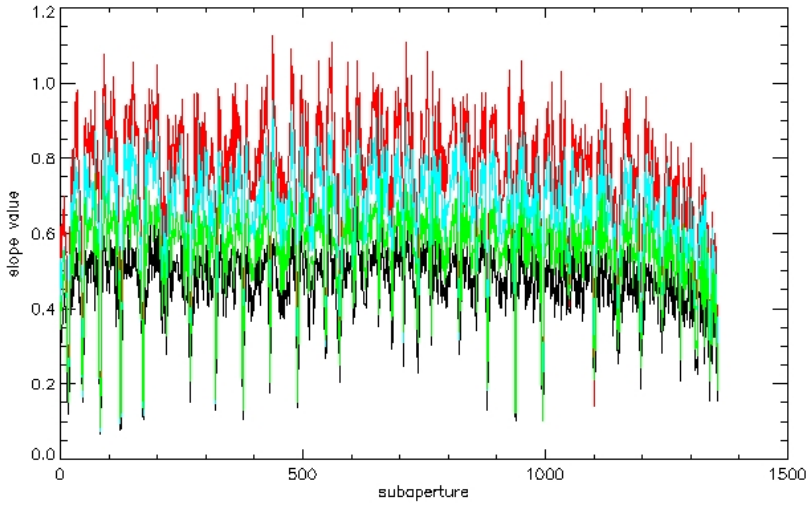

Figure 4.21: Evaluation of the average slope value detected by each subaperture on all integration time. Black: slopes signals detected at mod=16(λ/D), with a mean slope value of 0.45. Green: the slopes signals detected at mod=10(λ/D), with a mean slope value of 0.54. LightBlue: the slopes signals detected at mod=6(λ/D), with a mean slope value of 0.65. Red: the slopes signals detected at mod=3(λ/D), with a mean slope value of 0.75.

From figure 4.21 we can see that all the interaction matrices are inside the saturation range of the pyramid WFS (at about 0.75), and the results obtained by modulation 3(λ/D) and 6(λ/D) are also inside the linearity range. We can see a definite improvement of all the results. In order to proceed with the next step, we construct the pseudo-inverse of the interaction matrix measured by modulation 6(λ/D), that called IM_4.

STEP 4 CLOSED LOOP

Thanks to the REC of IM_4, we want to measure the 400 modes by using a REC matrix of 400 modes, this is the last step. The different modulations used are: mod=3(λ/D), and mod=2(λ/D), obtaining two different IM.

From figure 4.22, we can see that both the measures performed are inside

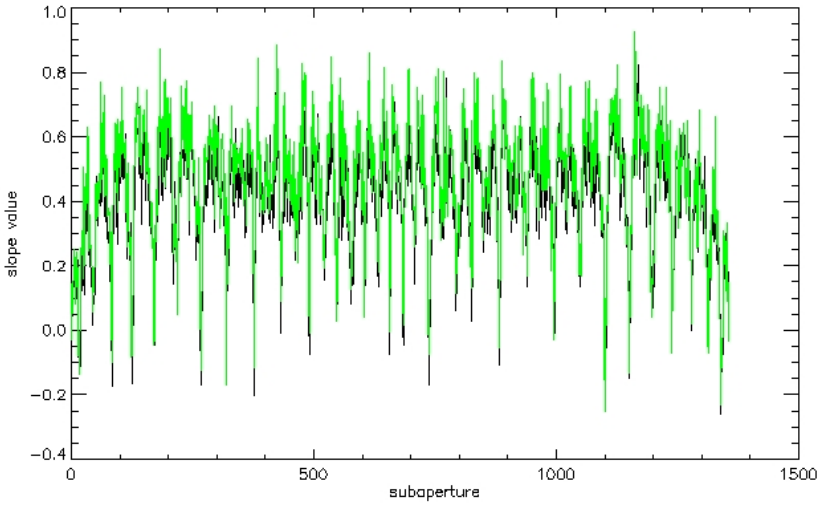

Figure 4.22: Evaluation of the average slope value detected by each subaperture on all integration time. Black: slopes signals detected at mod=3(λ/D), with a mean slope value of 0.40. Green: the slopes signals detected at mod=2(λ/D), with a mean slope value of 0.46.

both the pyramid WFS threshold of saturation and of linearity. So we have succeeded in our goal: the interaction matrix measured directly on sky with atmospheric turbulence.

In the figure 4.23 there is a schema of the measure procedure.

Analysis of the closed loop results

Point Spread Function (PSF) value

In order to check the results we have measured the psf on the image viewer, by closing the loop using two the reconstructor: one Rec is the pseudo-inverse of interaction matrix measured by the push-pull method in open loop calibration (without any kind of disturb during the loop), that we call Rec_{pp}, the other Rec is the pseudo-inverse of interaction matrix measured by applying the sinusoidal signal modulation method in closed loop calibration directly on sky (so with an atmospheric disturb injected), that we call Rec_{sin}; this last matrix is the result of the previous steps described. These measures are repeated multiple

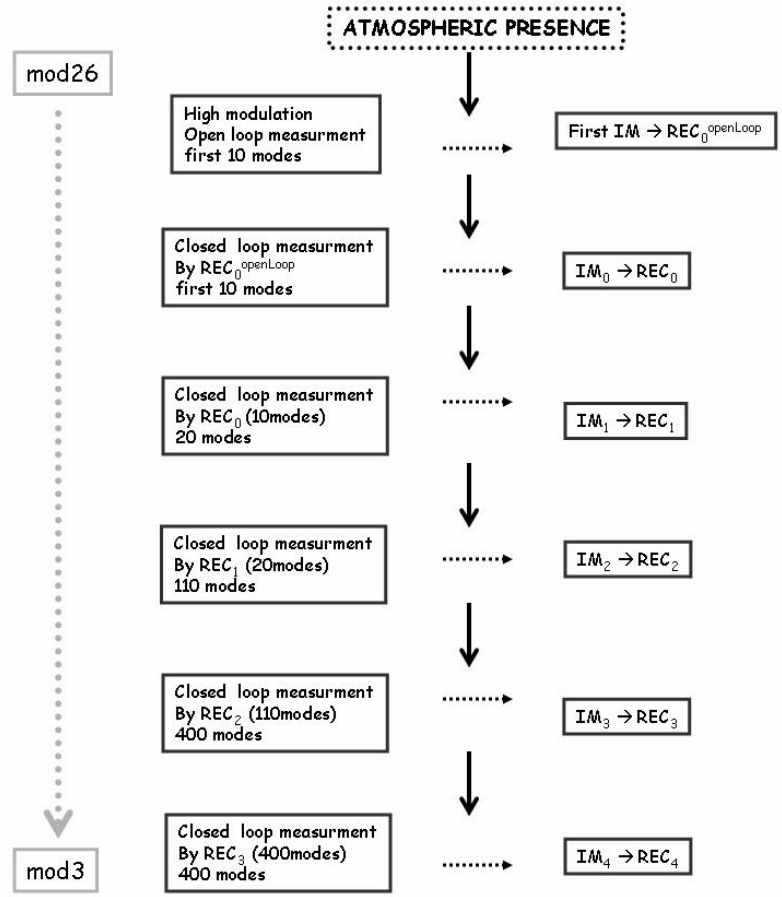

Figure 4.23: Schema of the simulation procedure in order to measure the IM in an atmospheric environment

times, because of the presence of some possible stochastic local disturb of the solar tower, like gusts of wind. In the next figures we can compare the best result obtain from the two sets of measures of each closed loop done (one set for each Rec used, 4.24), evaluating in H band with a magnitude star of 8.5, and TT modulation equal to 3. By the measures repeated we obtain a medium value of PSF of 80 percent for Rec_{pp} case, and 70 of PSF Rec_{sin}.
From these results we can see that the PSF Rec_{pp} are better than 10 percent respect to Rec_{sin}, but we can't forget that the first result is the one obtained by applying the reconstructor derived from a push pull open loop calibration, the other result is instead obtained by measuring the calibration matrix directly on sky, with atmospheric presence.

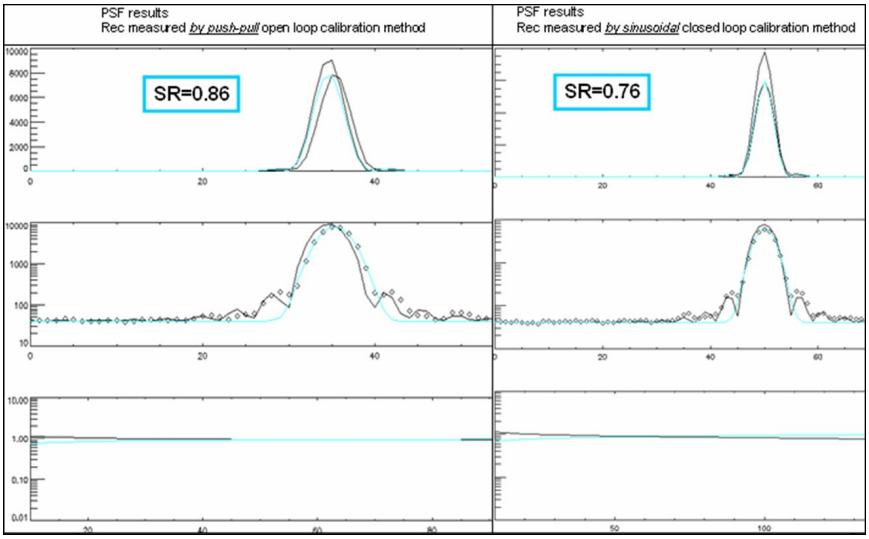

Figure 4.24: On the left box they are the results of PSF obtained by closing the loop using a reconstructor obtained by push-pull calibration method. The first plot: the comperison between the theoretical psf (black higher line), the measured psf (light blue line) and the result of fitting (black line near the light blue one). The second plot is the same of the previous one but in logarithmic scale: the theoretical psf (black higher line), the measured psf (dotted black line) and the result of fitting (light blue line). The third plot represents the strehl ratio as function of dimension of the box where we evaluate our psf result. So we have found a minimum dimension of the box over which the energy to calculate the theoretical psf, is invariant from box dimension, and so we obtain one unique SR result. In fact in this third plot we can see that, after an initial decreasing slope, the line is a straight line. On the right box are the results of PSF obtained by closing the loop using a reconstructor obtained by applying sinusoidal calibration method directly on sky (in closed loop operation system). The three plot are the same of the left box case.

Modal decomposition values

Another important check in order to evaluate the results obtained is the modal decomposition: for each single mode, we want to analyze the root mean square of residual on the WFS after the correction of the atmospheric turbulence. In the next figure (4.25) we analyze the same case of PSF evaluation, by closing the loop using both the reconstructor: Rec_{pp} and Rec_{sin}, in H band with a magnitude star of 8.5.

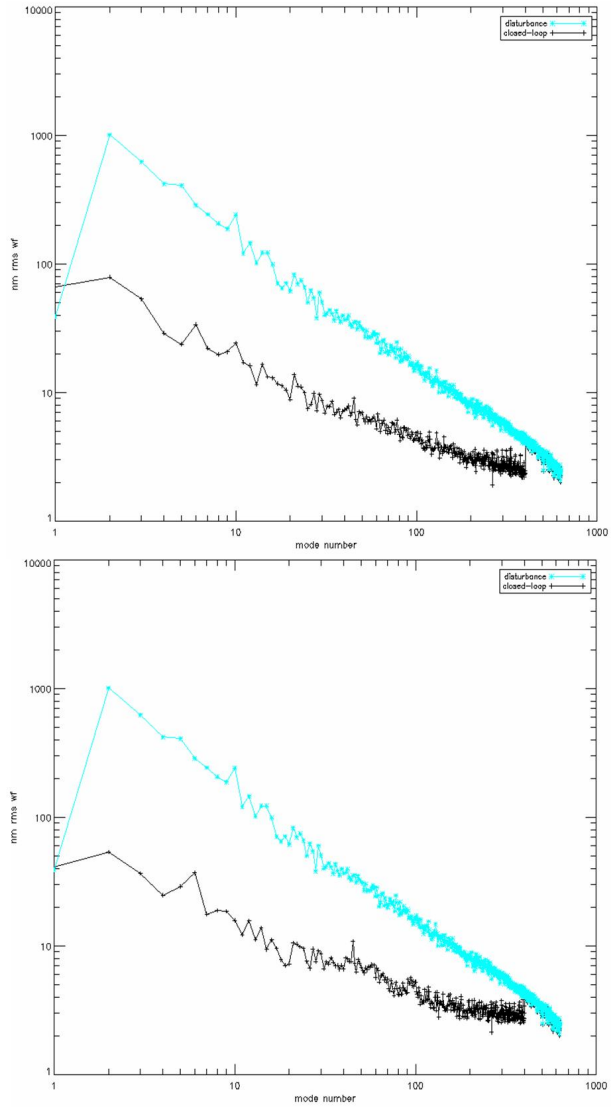

Figure 4.25: On the top: modal decomposition of closed loop residual by Rec_{pp}, black line is the residual value (nm unit) for each mode, light blue line is the atmospheric amplitude value detected for each mode (nm unit). On the bottom the same line valuated for the modal decomposition of closed loop by using Rec_{sin}.

From the figure 4.25 we can see that the results are similar, and in order to compare them, we plot the two results (root mean square of residual on the WFS after the correction of the atmospheric turbulence) together. We can see from figure 4.26 that the residuals evaluated using the Rec_{sin} (light blue line in this figure) are better than the one evaluated using the Rec_{pp} for about the first 50 modes , instead for the other modes it's the opposite.

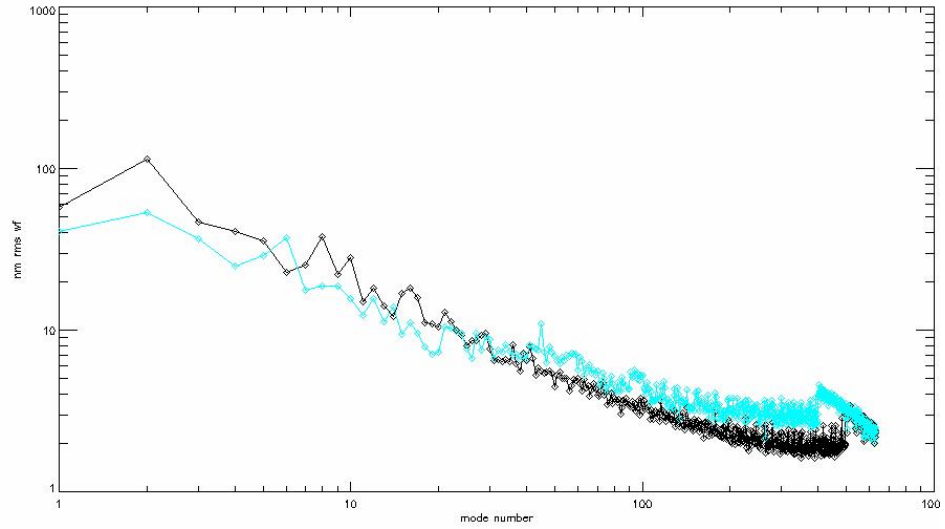

Figure 4.26: black line: modal decomposition of closed loop residual by Rec_{pp}; light blue line: modal decomposition of closed loop by using Rec_{sin}.

This suggest us to use the sinusoidal modulation method for calibrate the first 50 modes, and the push-pull method to calibrate the modes remainder, where the fiber-based IM measure is possible.

Chapter 5

Conclusion and future developments

The work done for this PhD thesis can be divided into two parts: the first regards the implementation of the AO LBT system and the second the study of a new method to calibrate the AO loop basically based on the possibility to measure the IM directly on sky.

1) About the first one it is convenient to highlight that the WFS board contains the pyramid sensor and all the optical elements required to work with it. I have spent part of my PhD on this optical board curing the optical alignments and testing some optical components.
Particularly I have worked on the behavior of the atmospheric dispersion corrector (ADC), comparing simulated results with the real ones. After some preliminary studies, like to find the right value of the refraction index of the glasses composing the two couple of prisms, the good agreement between simulations and measurements has been found out as consequence of its correct functionality. Only after this study it has been decided to implement the ADC inside the AO board of LBT.
I have verified the correct alignment of the optical WFS board itself and after this we have been able to test the whole LBT AO system in the Arcetri solar tower: an environment very similar to the one at the telescope has been reproduced, and the two mains subsystems of the LBT FLAO, the pyramid sensor and the secondary deformable mirror, have been tested for the first time

together in a realistic condition.

2) In the Arcetri Solar Tower Laboratory the second part of my PhD thesis work has been done. We have applied the sinusoidal calibration technique in order to measure the interaction matrix of the AO system, that is necessary in order to calculate the correct commands for the secondary deformable mirror actuators starting from the wavefront measurement realized using the pyramid based WFS.
We have used an auxiliary fiber source light measuring the IM in two cases: with no simulated turbulence(open loop operation of the AO system), and by injecting a disturbance "atmospheric like" (closed loop operation of the AO system). In this last case (the most important one) we measure the IM "directly" on sky, and we have obtained a strehl-ratio (at about 75 percent in H band). This value is comparable with the one obtained in open loop calibration, without any kind of injected atmospheric disturbances.

The results obtained in this Phd work measuring the IM directly in the Arcetri solar tower system are crucial for the future development: the possibility of the acquisition of IM directly on sky means that we are able to calibrate an AO system also for extremely large telescope class where classic IM measurements technique are problematic and, sometimes, impossible.
This technique (preliminarily used for the LBT AO calibration in the Arcetri Solar Tower laboratory) will be used during First Light AO LBT on Mt.Graham, with night-time commissioning scheduled for April 2010, and we expect that it will be possible to use this technique on Extremely Large class of future Telescopes.
Therefore the calibration is necessary in order to take care that an AO system would work correctly as an AO system is necessary in order to have the possibility to use a large telescope at its maximum possible resolution.
Finally we have not to forget the reason why we need this: the main aim is to observe the universe. Thanks to these new big class of telescopes and only using their full capabilities, we will be able to increase our knowledge of the

universe objects observed, because we will be able to resolve more detailed characteristics, discovering, analyzing and understanding the behaviour of the universe components.

In the last century the study of phenomena at early epochs in the expansion of the Universe has been very important for the astronomy. LBT, with its high resolution (i.e a near infrared beam (2μm) combiner which provides the diffraction limit of the full 22.8 meter baseline of 0.02 arc sec, and for a single primary mirror 8.4m a 2μm the angular resolution is 0.06 arc sec) can try to answer the questions of how the material content of the universe evolved from the big bang to the current distribution of galaxies, stars and planets of composition capable of supporting life. LBT will permit the identification of process formation of the galaxies, and also allow the analysis of their composition and radial motion . It will also give the possibility to study faint objects (like low mass stars or brown dwarfs) in the near stellar clusters. Furthermore, the high spatial resolution capability will also permit the study of high energy structure like galaxy nuclei, and the supermassive black holes which seem to power the quasars and radio sources. For example for an AGN at 4 Mpc of distance (i.e Circinus, a Seyfert Galaxy in the Circinus constellation), the central compact region requires in K-band (2.2μm) a resolution of 0.07" in order to resolve 1pc of object size scale; LBT at this IR wavelength arrives to a resolution about 0.02 arc sec.

This is a short picture of the importance of obtaining the best possible resolution in the telescope instruments, in order to obtain the best possible astrophysical results, and we can see now that the two things are complementary and have to proceed into the same direction.

Acronimi

ADC: atmospheric dispersion corrector
AGW: acquisition, guiding and wavefront
AO: adaptive optic
AS: adaptive secondary
CL: closed loop
DM: deformable mirror
ELT: extremely large telescope
LBT: large binocular telescope
FFT: fast Fourier transform
FLAO: first light adaptive optic
FOV: field of view
IM: interaction matrix
OL: open loop
PM: primary mirror
PS: pyramid sensor
PSF: point spread function
REC: reconstructor
RMS: root mean square
SDM: secondary deformable mirror
TT: tip-tilt
WFS: wavefront sensor

Bibliography

[S. Esposito & al. 2006] S. Esposito, R. Tubbs, A. Puglisi, S. Oberti, A. Tozzi, M. Xompero, and D. Zanotti : High SNR measurement of interaction matrix on-sky and in lab, in Advances in Adaptive Optics II, B. L. Ellerbroek and D. Bonaccini Calia, eds., vol. 6272 of Proc. SPIE, p. 62721C, July 2006.

[M.Kasper & al. 2004] M. Kasper, E. Fedrigo, D. P. Looze, H. Bonnet, L. Ivanescu, and S. Oberti :Fast calibration of high-order adaptive optics systems, Optical Society of America Journal A, 21, pp. 1004-1008, 2004.

[S.Stroebele & al. 2006] S. Stroebele, R. Arsenault, D. Bonaccini Calia, R. D. Conzelmann, B. Delabre, R. Donaldson, M. Duchateau,S. Esposito, E. Fedrigo, W. K. P. Hackenberg, N. N. Hubin, M. Le Louarn, S. Oberti, R. Stuik, and E. Vernet:The ESO adaptive optics facility , in Advances in Adaptive Optics II, Ellerbroeck B. and Bonaccini Calia D., ed., 6272, in publication 2006.

[F.P. Wildi & al.2004] F.P. Wildi and G. Brusa: Determining the interaction matrix using starlight, in Advancements in Adaptive Optics, D. Bonaccini Calia, B. L. Ellerbroek, and R. Ragazzoni, eds., 5490, pp. 164-173, 2004.

[S. Oberti & al.2006] S. Oberti, R. Muradore, S. Esposito, R. Arsenault, E. Fedrigo, M. E. Kasper, J. Kolb, E. Marchetti, F. Quiros-Pacheco, and C. Soenke: Large DM AO systems: synthetic IM or calibration on sky?, in Advancements in Adaptive Optics, D. Bonaccini Calia, B. L. Ellerbroek, and R. Ragazzoni, eds., 6272, in publication 2006.

[F.Pieralli & al.2008] F. Pieralli, A. Puglisi, F. Quiros Pacheco, and S. Esposito, Sinusoidal calibration technique for Large Binocular Telescope system, in Adaptive Optics Systems, N. Norbert Hubin, E. M. Claire, and P. L. Wizinowich, eds., vol. 7015 of Proc. SPIE, p. 70153A, July 2008.

[S.Esposito & al.2006] S. Esposito, A. Tozzi, A. Puglisi, E. Pinna, A. Riccardi, S. Busoni, L. Busoni, P. Stefanini, M. Xompero,D. Zanotti, and F. Pieralli: First light AO system for LBT: toward on-sky operation, in Advances in Adaptive Optics IIi, B. L. Ellerbroek and D. Bonaccini Calia, eds., vol. 6272 of Proc. SPIE, July 2006.

[H.Mandel & al.2001] Mandel H. a, Appenzeller I. a, Bomans D. d, Eisenhauer F. et al .: LUCIFER - a NIR Spectrograph and Imager for the LBT,Proc. SPIE, vol. 40008,p.767-777,(2001),Optical and IR instrumentation and Detectors, Masanori Iye; Alan F.Moorwood;Eds.

[S.Esposito & al.2003] S. Esposito, A. Tozzi, A. Puglisi, L. Fini, P. Stefanini, P. Salinari, D. Gallieni, and J. Storm, Development of the first light AO system for the large binocular telescope, in Astronomical Adaptive Optics Systems and Applications. Edited by Tyson, Robert K.; Lloyd Hart, Michael., SPIE Proc. 5169, pp. 149,158, Dec. 2003.

[S.Esposito & al.2003] S. Esposito, A. Tozzi, D. Ferruzzi, M. Carbillet, A. Riccardi, L. Fini, C. Vérinaud, M. Accardo, G. Brusa, D. Gallieni, R. Biasi, C. Baffa, V. Biliotti, I. Foppiani, A. Puglisi, R. Ragazzoni, P. Ranfagni, P. Stefanini, P. Salinari, W. Seifert, and J. Storm, First Light Adaptive Optics System for Large Binocular Telescope, in Adaptive Optical System Technologies II. Edited by Wizinowich, Peter L.; Bonaccini, Domenico, vol. 4839 of Proc. SPIE, pp. 164-173, Feb. 2003.

[J.Storm & al.2000] J. Storm, W. Seifert, S. Bauer, F. Dionies, U. Hanschur, J. M. Hill, G. Moestl, P. Salinari, W. Varava, and H. Zin-

necker, Wavefront sensing and guiding units for the Large Binocular Telescope, SPIE Proc. 4007,pp. 461,469, July 2000.

[A.Riccardi & al.2004] A. Riccardi, G. Brusa, M. Xompero, D. Zanotti, C. Del Vecchio, P. Salinari, R. Biasi, M. Andrighettoni,D. Gallieni, S. Miller , P. Mantegazza:The adaptive secondary mirrors for the Large Binocular Telescope: a progress report, Proc S.P.I.E. 2004, 5490, pp. 1564-1571.

[D.Gallieni & al.2003] D. Gallieni, E. Anaclerio, P.G. Lazzarini, A. Ripamonti, R. Spairani, C. Del Vecchio, P. Salinari, A. Riccardi, P.Stefanini, LBT adaptive secondary units final design and construction, Astronomical Telescope and Intrumentation, 2003, SPIE.4839, 765G.

[A.Tozzi & al.2008] A. Tozzi, P.Stefanini, E. Pinna, S.Esposito:The Double Pyramide wavefront sensor for LBT, Proc. of SPIE Vol.7015, 701558,1 (2008)

[R.Ragazzoni.1996] R. Ragazzoni, Pupil plane wavefront sensing with an oscillating prism, J. Mod. Opt. 43, pp. 289-293, 1996.

[A.Tozzi 2003] A. Tozzi, The LBT light source, FLAO LBT document 687f100.

[A.Filippenko 1982] A. Filippenko: The importance of atmospheric differential refraction in spectrophotometry,PASP 94, pp. 715,721, 1982.

[C.G Wynne 1997] C. G. Wynne, Atmospheric dispersion in very large telescopes with adaptive optics,Mon. Not. R. Astron.Soc. 285, 130,134 (1997).

[A:N.Kolmogorov 1991] A. N. Kolmogorov: The local structure of turbulence in incompressible viscous fluid for very large Reynolds numbers (translation). Proceedings of the Royal Society of London. Series A, 434(1890):9,13, 1991.

[A.Tozzi & al. 2003] A. Tozzi,F.Pieralli, W2 Pupil Rerotator, FLAO LBT document number:687f006,2003.

[F.Quirós & al. 2009] F. Quirós-Pacheco,L.Busoni : FLAO system baseline and goal performance, FLAO LBT document number: ,2009.

[F.Quirós2009] F. Quiros-Pacheco: FLAO system tests in Arcetri: Phase A final report, LBT technical report, 02 Dec 2009.

[A.Burvall & al. 2006] A.Burvall, E.Daly, S.R. Chamot,C.Dainty: Linearity of the pyramid wavefront sensor. Opt. Express 14, 11925-11934 (2006) .

[S.Esposito & al. 2000] S. Esposito, O. Feeney, and A. Riccardi : Laboratory test of a pyramid wavefront sensor. In Adaptive Optical Systems Technology, P. L. Wizinowich, ed., vol. 4007 of Proc. SPIE, pp. 416,422, July 2000

[S.Esposito & al. 2009] S.Esposito,G.Brusa, L.Busoni: FLAO system test plan in solar tower, document number:FLAO05,2009.

[Kolmogorov, 1941] Kolmogorov, A. N. (1941): The local structure of turbulence in incomressible viscous fluids for very large reynolds numbers. Compt. Rend.Acad. Sci. (SSSR), 30, 301.

[Fried, 1966] Fried, D. L. (1966): Optical resolution through a randomly inhomogeneous medium for very long and very short exposures. J. Opt. Soc. Am., 56,(1372,1379).

[A.Riccardi & al. 2004] Riccardi, A., Brusa, G., Xompero, M., Zanotti, D., Del Vecchio, C., Salinari, P., Ranfagni, P., Gallieni,D., Biasi, R., Andrighettoni, M., Miller, S., and Mantegazza, P.: The adaptive secondary mirrors for the Large Binocular Telescope: a progress report., Proc. SPIE 5490, 1564,1571 (2004).

[C.Del Vecchio & al. 2004] Del Vecchio, C., Miglietta, L., and Davison, W. B.: Mechanical design of the Large Binocular Telescope, Proc. SPIE 2199, 773,782 (June 1994).

[J.Hill & al. 2008] Hill, J. M., Green, R. F., Slagle, J. H., Zappelini, G. B., Brynnel, J., Cushing, N. J., Little, J., and Wagner,R. M.: The large binocular telescope, Proc. SPIE 7012, 2 (2008).

[S.esposito & al. 2001] S. Esposito and A. Riccardi: Pyramid wavefront sensor behavior in partial correction adaptive optic systems. Astronomy and Astrophysics,369(2):L9-L12, 2001.

[W.H. Southwell 1980] W. H. Southwell: Wave-front estimation from wave-front slope measurements. JOSA, 70:998-1006, 1980.

[R. J. Noll 1976] R. J. Noll: Zernike polynomials and atmospheric turbulence. JOSA, 66(3):207-211, 1976.

[S. C. West & al. 2002] S. C. West, S. P. Callahan, D. L. Clark, B. Cuerden, D. G. Fabricant, D. Fisher, C. B. Foltz, J. D. Gibson, W. L. J. Kindred, H. M. Martin, D. L. McKenna, B. A. McLeod, T. E. Pickering, P. F. Spencer, T. J. Trebisky, K. Van Horn, and T. Williams, J: status of the 6.5m conversion of the multiple mirror telescope since 2000 may, Proc. SPIE 4837, 2002.

[A.Riccardi & al. Feb. 2003] A. Riccardi, G. Brusa, P. Salinari, D. Gallieni, R. Biasi, M. Andrighettoni, and H. M. Martin: Adaptive secondary mirrors for the Large Binocular Telescope, in Adaptive Optical System Technologies II. Edited by Wizinowich, Peter L.; Bonaccini, Domenico, SPIE Proc. 4839, pp. 721,732, Feb. 2003.

[A.Riccardi & al. Dec. 2003] A. Riccardi, G. Brusa, P. Salinari, S. Busoni, O. Lardiere, P. Ranfagni, D. Gallieni, R. Biasi, M. Andrighettoni, S. Miller, and P. Mantegazza: Adaptive secondary mirrors for the Large binocular telescope, in Astronomical Adaptive Optics Systems and Applications. Edited by Tyson, Robert K.; Lloyd Hart, Michael, SPIE Proc.5169, pp. 159,168, Dec. 2003

[P.Salinari & al. 1993] P. Salinari, C. Del Vecchio, and V. Biliotti: study of an adaptive secondary mirror, in Active and adaptive optics. F. Merkle, ed., Proc. ICO16 Satellite Conference 48, pp.

247,253, International Commission for Optics (ICO), (Garching, Germany), 1993.

[E.Masciadri & al. 2010] E. Masciadri, J. Stoesz, S. Hagelin1, F. Lascaux: Optical turbulence vertical distribution with standard and high resolution at Mt. Graham, arXiv:1001.1304, 2010.

[M.Schoeck & al. 2009] Schoeck, M., Els, S., Riddle, R., Skidmore,W., Travouillon,T., Blum, R., Busots, E., Chanan, S.G., Djorgovski, S.G.,Gillet, P., Gregory, B, Nelson, J., Ot´arola, A., Seguel,J., Vasquez, A., Walker, A., Walker, D., Wang, L. 2009,PASP, 121, 878, 384

Acknowledgements

Eccoci, siamo alla fine di questa esperienza di dottorato...
Siceramente? si, proprio bella. Ad oggi sono contentissima di averne avuto la possibilità, indipendentemente. Ho imparato veramente molte cose, scientifiche e umane.
Grazie Arcetri, perchè ho incontrato persone che sono state comunque in grado di arricchirmi, anche senza minimamente accorgersene. Grazie a tutte loro per avermi fatto continuamente confrontare con me stessa, con le mie capacità e a lottare continuamente per ottenere.
Grazie a tutte le persone che in questi tre anni hanno avuto a che fare con me, e, sia in silenzio sia con le parole, sia con il confronto che non, sia per poco che ripetutamente, sia nel bene che nel male, sono comunque riuscite a comunicarmi dei valori importanti, a rendermi ben visibile la persona che voglio diventare e le cose che sono bramosa di imparare.
Un grazie particolare va ad Alfio, che è l'esempio evidente di come una laurea non sia sinonimo di cultura. Un amico, oltre che un degno collega, che senza chiedergli mai niente mi ha sempre spontaneamente aiutato, e soprattutto ha sempre creduto nelle mie capacità, cosa che mi ha dato non poca forza, lui lo sa. Un'altra persona che mi sento veramente di ringraziare è Andrea, uno degli esseri più colti e capaci che conosca, e la cosa che lo rende unico è che lo fa con una umiltà che non ha eguali (altro segno di intelligenza estrema). Andrea è un amico, è sinomino di apertura mentale, di rispetto, di buon esempio umano.
Grazie Bologna per avermi dato la possibilità di continuare a seguire l'Astrofisica in tutti i suoi aspetti generali, seguendone gli aggiornamenti.
Il lavoro di questa tesi è frutto di una conoscenza che prima di questi tre anni non avevo, e che rimarrà mia per sempre. Lo trovo bellissimo.
Grazie alla mia famiglia, tutta, perchè parte di me. Mamma, babbo, ci siamo

arrivati. Piccola Giulina un giorno te la farò leggere.
Grazie Arcetri, perchè mi hai fatto incontrare Alessandro, con i cui occhi vedo un mondo privo di aberrazioni, senza il bisogno di nessun sistema di correzione.
Grazie Ale, perchè con te ho voglia di vederlo, questo mondo.
Grazie Franci, sei stata in gamba.